Engineering Structures 315 (2024) 118429

Contents lists available at ScienceDirect

Engineering Structures

journal homepage: www.elsevier.com/locate/engstruct

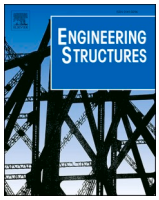

Ductile design of single-pier steel and concrete hybrid coupled walls with hinged base and corner components

Fabrizio Scozzese [a,*], Nicola Ceccolini [a], Alessandro Zona [a], Andrea Dall'Asta [a], Hervé Degée [b]

[a] School of Architecture and Design, University of Camerino, Ascoli Piceno, Italy
[b] Construction Engineering Research Group, Hasselt University, Hasselt, Belgium

ARTICLE INFO

Keywords:
Steel and concrete hybrid structures
Steel structures
Dissipative links
Seismic design
Seismic-resistant structures

ABSTRACT

The seismic behaviour of hybrid coupled walls (HCWs) made of a single reinforced concrete (RC) wall connected to two steel side columns through steel links, named as single-pier HCWs (SP-HCWs), is studied through nonlinear finite element simulations. The design concept is that the steel links are intended to work as dissipative elements while the steel side columns and the RC wall should remain elastic. Given that previous studies highlighted difficulties in avoiding damage at the base of the RC wall due to the concentration of bending moment, this study focuses on a special configuration providing very limited damage at the base of the RC wall that could be rapidly and economically repaired. The original scheme of SP-HCW with fixed base is modified introducing a hinged connection combined with vertical steel elements, called corner components. A ductile design methodology is proposed and applied for proportioning 54 case studies with different building heights, coupling ratios, height-to-length ratios of the RC wall, in addition to different base conditions (fixed base, hinged base with corner components designed as non-dissipative elements, hinged base with corner components designed as dissipative elements). Results of nonlinear finite element analyses validate the design methodology and highlight the potentialities of the proposed solutions, showing the benefits of a hinged base with corner components.

1. Introduction

The term hybrid coupled wall (HCW) commonly refers to two reinforced concrete (RC) walls connected by means of steel coupling beams or steel-concrete composite coupling beams, e.g. [1–5], as depicted in Fig. 1a. The walls are subjected to bending, shear, and an alternation of tension and compression axial forces while the coupling beams are subjected to bending and shear; the resulting stiffness and strength are greater than the summation of the contributions of the individual uncoupled walls. HCW were conceived as an evolution of RC coupled walls, e.g. [6–8], to better exploit the stiffness and shear strength of simple RC walls [9], given the more stable hysteretic behaviour of the steel links as well as their possible replacement if damaged [10]. More recently, a different configuration for HCWs was developed within a European research project [11], and further studied in subsequent works [12–17]: a single RC wall is coupled to two steel side columns through steel links working as dissipative elements (Fig. 1b). Pinned connections are used between the links and the side columns while the connections of the links to the RC wall transfer both shear and bending moment. The RC wall is subjected to bending (plus a constant and small axial force from permanent loads) while the side steel columns are subject to an alternation of compression and traction (plus small bending moments due to the eccentricity of the connections with the links). The damaged steel links can be replaced after a seismic event, provided that a suitable connection detailing is used, as those proposed and tested in [11] and [18]. Compared to conventional HCWs made by two RC walls, the proposed innovative single-pier HCW (termed as SP-HCW hereafter) is expected to provide a major benefit: the RC wall is subjected to bending only leading to a more efficient control of the damage, given that no additional alternate traction-compressions forces are applied. In addition, a smaller floor space is expected due to the smaller size of one RC wall plus two steel side columns with respect to two RC walls.

In the seismic design of SP-HCWs, three critical aspects require attention: base shear level providing the activation of the dissipative mechanisms in the links; intensity of the damage expected at the base of the RC wall; intensity of the traction forces in the foundations transferred by the side steel columns. Such aspects are strongly intercorrelated, depending on design parameters related to the geometry, stiffness,

* Corresponding author.
E-mail address: fabrizio.scozzese@unicam.it (F. Scozzese).

https://doi.org/10.1016/j.engstruct.2024.118429
Received 4 April 2023; Received in revised form 15 April 2024; Accepted 9 June 2024
Available online 21 June 2024

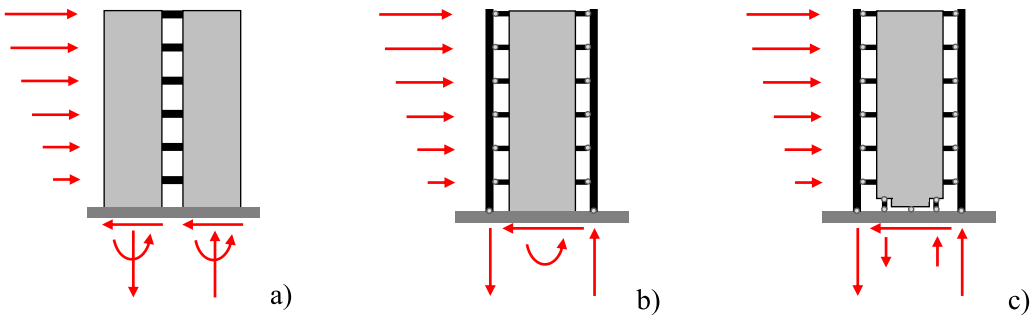

Fig. 1. Scheme and base reactions under horizontal loads for: a) HCW; b) SP-HCW; c) SP-HCW with hinged base and corner components.

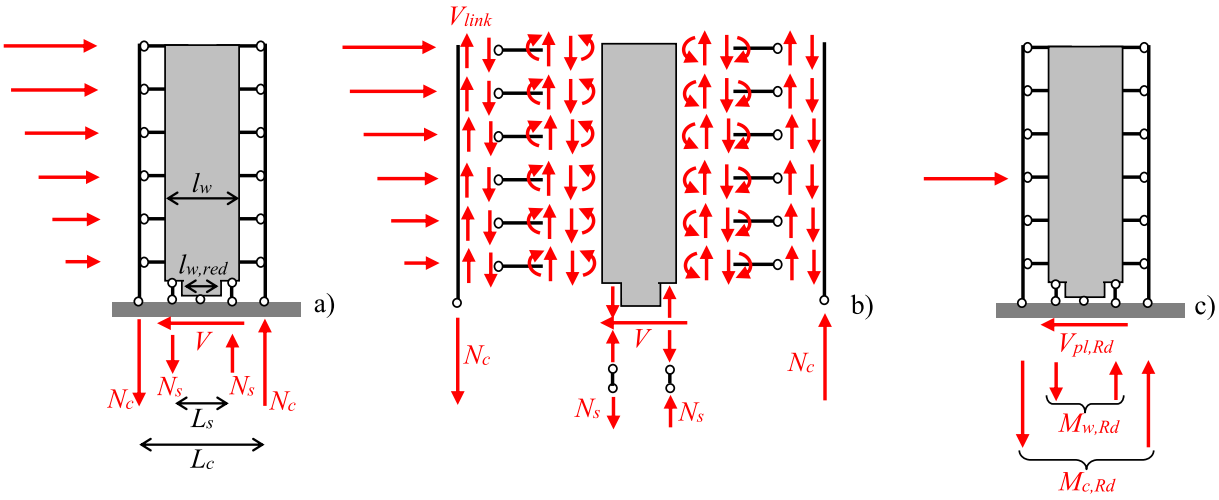

Fig. 2. Resisting mechanism in the SP-HCW with hinged base and corner components under horizontal loads: a) base reactions; b) internal forces in the components; c) fully developed plastic mechanism at the base.

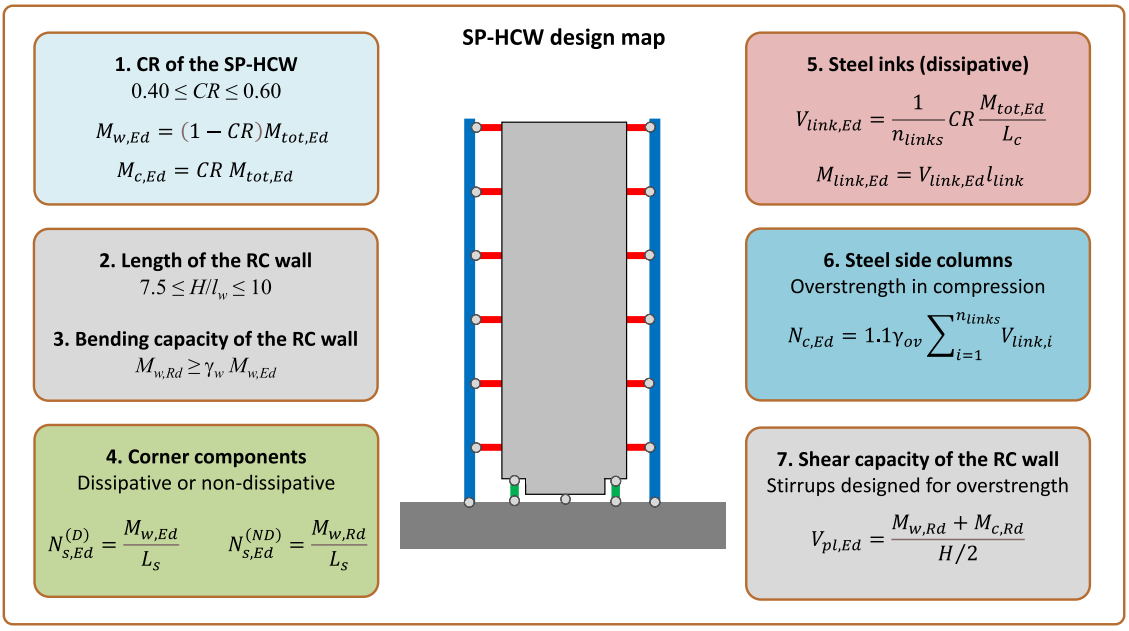

Fig. 3. Graphical summary of the proposed design procedure (nomenclature defined in the text).

and strength of the system components. For example, an increment in the amount of bending moment assigned at the base of the RC wall with respect to the bending moment resisted by the side columns gives a reduction of the traction forces in the foundations. However, a larger bending moment assigned to the RC wall leads to the increment of its lateral stiffness with respect to those of the steel links, and postpones

Table 1
List of the designed case studies.

Storeys	H/l_w	Corner components	CR	Label
3	7.5	No corner components	0.40	S3W75CR40
			0.50	S3W75CR50
			0.60	S3W75CR60
		Dissipative	0.40	S3W75CR40-CCD
			0.50	S3W75CR50-CCD
			0.60	S3W75CR60-CCD
		Non-dissipative	0.40	S3W75CR40-CCND
			0.50	S3W75CR50-CCND
			0.60	S3W75CR60-CCND
	10	No corner components	0.40	S3W100CR40
			0.50	S3W100CR50
			0.60	S3W100CR60
		Dissipative	0.40	S3W100CR40-CCD
			0.50	S3W100CR50-CCD
			0.60	S3W100CR60-CCD
		Non-dissipative	0.40	S3W100CR40-CCND
			0.50	S3W100CR50-CCND
			0.60	S3W100CR60-CCND
6	7.5	No corner components	0.40	S6W75CR40
			0.50	S6W75CR50
			0.60	S6W75CR60
		Dissipative	0.40	S6W75CR40-CCD
			0.50	S6W75CR50-CCD
			0.60	S6W75CR60-CCD
		Non-dissipative	0.40	S6W75CR40-CCND
			0.50	S6W75CR50-CCND
			0.60	S6W75CR60-CCND
	10	No corner components	0.40	S6W100CR40
			0.50	S6W100CR50
			0.60	S6W100CR60
		Dissipative	0.40	S6W100CR40-CCD
			0.50	S6W100CR50-CCD
			0.60	S6W100CR60-CCD
		Non-dissipative	0.40	S6W100CR40-CCND
			0.50	S6W100CR50-CCND
			0.60	S6W100CR60-CCND
9	7.5	No corner components	0.40	S9W75CR40
			0.50	S9W75CR50
			0.60	S9W75CR60
		Dissipative	0.40	S9W75CR40-CCD
			0.50	S9W75CR50-CCD
			0.60	S9W75CR60-CCD
		Non-dissipative	0.40	S9W75CR40-CCND
			0.50	S9W75CR50-CCND
			0.60	S9W75CR60-CCND
	10	No corner components	0.40	S9W100CR40
			0.50	S9W100CR50
			0.60	S9W100CR60
		Dissipative	0.40	S9W100CR40-CCD
			0.50	S9W100CR50-CCD
			0.60	S9W100CR60-CCD
		Non-dissipative	0.40	S9W100CR40-CCND
			0.50	S9W100CR50-CCND
			0.60	S9W100CR60-CCND

link yielding, hence, reducing the dissipation capacity under seismic actions. Previous numerical studies [12–17] highlighted the global ductility of SP-HCWs and how it is influenced by various design parameters. Nevertheless, it was also pointed out that inelastic deformations could not be restricted to the steel links and would spread at the base of the RC wall, leading to costly damages not easy to be repaired. Hence, solutions able to avoid damage in the RC wall or, at least, allowing its fast and affordable repair, are very important to foster the possible use SP-HCWs as a compelling structural system. In this context, the objective of this study is to explore a design solution where the base of the RC wall is modified through the interposition of replaceable steel elements called corner components [19] combined with a hinged restrain at the base, as depicted in Fig. 1c. Corner components were the object of some recent experimental and numerical studies that showed their effect in increasing resilience when adopted in RC walls and classical HCWs, e.g., [20–25], and their unexplored application to SP-HCWs appears very promising.

In this work, a design procedure for SP-HCWs with fixed base or hinged base with corner components is proposed revisiting the approach originally presented in [12], comparisons are made between the designs of a set of 54 case studies with fixed base and hinged base with corner components, nonlinear finite element simulations are illustrated and discussed for the designed case studies to provide insight into their expected seismic performance as well as into the potentialities of the use of corner components in SP-HCWs. The primary original contribution of this work is the introduction of corner components in SP-HCWs with the aim of avoiding seismic damage at the base of the RC wall more effectively as compared to previous attempts based on wall overstrength, hence, increasing resiliency in the proposed structural solution. Two different design approaches are explored, i.e., corner components designed as elements protecting the RC wall that do not participate with the primary dissipative mechanism, corner components designed to be part of the primary dissipative mechanism together with the steel links connecting the side steel columns to the RC wall. However, the contribution of this study is not solely the introduction of corner components, in fact, there are other novelties of this study that are significant advancements for SP-HCWs with fixed base. The design procedure, although apparently similar to the one previously proposed [12], is revised to achieve the same nominal capacity regardless the ratio taken between the contribution of the side steel columns with respect the total capacity to resist horizontal actions. In addition, the effect of the geometric height-to-length ratio of the RC wall is explored to move the suggested geometries towards slightly larger RC walls allowing less congestion in the rebar detailing, a possible problem highlighted in previous studies [11–15].

2. Ductile design of SP-HCWs with hinged base and corner components

2.1. Resisting mechanism to horizontal loads and coupling ratio

Horizontal loads in SP-HCW produce the forces and moments at the base depicted in Fig. 1b. The ratio between the moment $M_c = L_c N_c$ contributed by the two side columns and the total base moment ($M_{tot} = M_c + M_w$) is called coupling ratio (CR):

$$CR = \frac{M_c}{M_c + M_w} = \frac{M_c}{M_{tot}} = \frac{L_c N_c}{M_{tot}} \tag{1}$$

where M_w is the moment acting at the base of the RC wall, L_c is the lever arm of the two side steel columns and N_c is the axial force at the base of the side columns, equal to the summation of the shear forces $V_{link,i}$ ($i = 1, \ldots, n_{links}$) in the links:

$$N_c = \sum_{i=1}^{n_{links}} V_{link,i} \tag{2}$$

with n_{links} the number of links in each side.

In the case of hinged base and corner components (Fig. 1c and Fig. 2), $M_w = N_s L_s$ is provided by the corner components (N_s is their axial force and L_s is their lever arm). Accordingly, the coupling ratio can be rewritten as:

$$CR = \frac{L_c N_c}{L_c N_c + L_s N_s} \tag{3}$$

As previously assumed [11,12], the axial forces in the links are small and their effect is neglected (this is the case when gravity-resisting structures are connected directly to the RC wall and not to the side steel columns, in addition to construction sequences studied to avoid horizontal forces as those induced by concrete shrinkage).

2.2. Design procedure

The procedure for the design of SP-HCW presented in [12] is

Table 2
Designed RC walls (geometry and bending).

Label	l_w (cm)	b_w (cm)	$M_{w,Ed}$ (kNm)	Rebars (confined / non-confined areas)	Rebar geometric ratio (confined / non-confined areas, %)	$\Omega_{wall,M}$
S3W75CR40	140	44	1540.20	4ϕ26 + 18ϕ22 / -	1.45 / -	1.54
S3W75CR50		40	1283.50	4ϕ22 + 18ϕ20 / -	1.28 / -	1.50
S3W75CR60		36	1026.80	4ϕ20 + 18ϕ18 / -	1.16 / -	1.54
S3W100CR40	105	44	1540.20	4ϕ30 + 18ϕ28 / -	3.01 / -	1.56
S3W100CR50		40	1283.50	4ϕ28 + 18ϕ24 / -	2.52 / -	1.50
S3W100CR60		36	1026.80	4ϕ24 + 18ϕ22 / -	2.29 / -	1.53
S6W75CR40	280	44	3952.20	4ϕ26 + 8ϕ22 / 12ϕ12	1.78 / 0.72	1.59
S6W75CR50		40	3293.50	4ϕ22 + 8ϕ20 / 12ϕ12	1.53 / 0.65	1.54
S6W75CR60		36	2634.80	4ϕ22 + 8ϕ16 / 12ϕ12	1.32 / 0.60	1.59
S6W100CR40	210	44	3952.20	4ϕ26 + 10ϕ26 / 8ϕ16	2.56 / 1.51	1.55
S6W100CR50		40	3293.50	4ϕ26 + 10ϕ22 / 8ϕ14	2.24 / 1.31	1.51
S6W100CR60		36	2634.80	4ϕ24 + 10ϕ20 / 8ϕ12	2.08 / 1.20	1.58
S9W75CR40	420	44	7915.80	4ϕ26 + 8ϕ24 / 24ϕ14	1.98 / 0.58	1.54
S9W75CR50		40	6596.50	4ϕ24 + 8ϕ20 / 24ϕ14	1.64 / 0.54	1.50
S9W75CR60		36	5277.20	4ϕ20 + 8ϕ18 / 24ϕ14	1.38 / 0.52	1.55
S9W100CR40	315	44	7915.80	4ϕ28 + 10ϕ28 / 20ϕ16	2.97 / 1.19	1.58
S9W100CR50		40	6596.50	4ϕ26 + 10ϕ24 / 20ϕ14	2.52 / 1.01	1.50
S9W100CR60		36	5277.20	4ϕ24 + 10ϕ22 / 20ϕ12	2.36 / 0.91	1.55

hereafter reformulated and extended to the considered SP-HCWs with hinged base and corner components. This revision is based on the experience gained in this and in previous researches on SP-HCWs, considering the framework given in Eurocode 8 [26] as well as the indications in [27,28]. A design map summarizing the design steps is depicted in Fig. 3 to provide a graphical overview of the proposed dimensioning process.

The first step is the choice of CR, required to compute the demand in terms of base moments $M_{w,Ed}$ and $M_{c,Ed}$ in the RC wall and in the steel side columns, respectively, starting from $M_{tot,Ed}$, the total moment demand at the base:

$$M_{w,Ed} = (1 - CR) M_{tot,Ed} \tag{4}$$

$$M_{c,Ed} = CR\, M_{tot,Ed} \tag{5}$$

with recommended values in the range $0.40 \leq CR \leq 0.60$ for a shared engagement of the contributions of the steel and RC components to the resisting mechanism. In fact, values of CR lower than 0.40 result in a SP-HCW where the RC wall oversees the main contribution in resisting horizontal actions and the side steel columns have a secondary importance, making its structural behaviour similar to that of a single RC shear wall. On the other hand, values of CR higher than 0.60 lead to a secondary role of the RC wall, leaving to the steel columns the duty of resisting most of the horizontal actions. These extreme upper and lower regions of CR provide less efficient designs, as already highlighted in previous studies [11,12,14,15].

The second step is the definition of the length l_w of the RC wall (Fig. 2a). In the case of RC wall continuous to the foundation (no hinged base and no corner components adopted), previous researches [11,12] suggested the ratio $H/l_w = 10$ with H the total height of the wall, as possible optimal solution between the opposite needs of allowing sufficient horizontal displacements to activate plastic deformation in the steel links while preserving structural integrity and avoiding unfavourable second-order effects. However, given that the ratio $H/l_w = 10$ might result in designs with detailing difficulties in the reduced section at the hinged base when corner components are used, a larger RC wall length (ratio $H/l_w = 7.5$) is also explored in this study.

The third step is the definition of the width b_w of the RC wall and the design of its longitudinal reinforcing steel bars to provide adequate bending strength $M_{w,Rd}$. Specifically, a margin should be assigned to the bending resistance to control damage in the RC wall; in this study the enforced condition is $M_{w,Rd} \geq \gamma_w M_{w,Ed}$ with $\gamma_w = 1.5$ as recommended in [12] based on the results of numerical simulations.

The fourth step in the design specifically concerns the new solution investigated in this study, involving a base hinge and two corner components. Once the geometry of the RC wall is set, the lever arm $L_s < l_w$ of the steel corner component (Fig. 2a) is known and, consequently, the demand of axial force $N_{s,Ed}$ in the corner components can be determined. Two alternative design options for the corner components are explored in this study: in the first one the axial force is computed from $M_{w,Ed}$ as:

$$N_{s,Ed}^{(D)} = \frac{M_{w,Ed}}{L_s} = (1 - CR)\frac{M_{tot,Ed}}{L_s} \tag{6}$$

and, hence, no overstrength is adopted in the design of the corner components that are expected to yield and dissipate energy; in the second one the axial force is computed from $M_{w,Rd} \geq \gamma_w M_{w,Ed}$ as:

$$N_{s,Ed}^{(ND)} = \frac{M_{w,Rd}}{L_s} \tag{7}$$

and, consequently, the same overstrength of the wall is transferred to the corner components. In this second option the corner components are designed as non-dissipative elements as is the RC wall. In both design options, stocky elements, e.g., components with generalized slenderness $\bar{\lambda} \leq 0.2$ and class 1 compact cross-section according to Eurocode 3 [29], are recommended. A possible alternative is the use of buckling-restrained braces, e.g., [22].

The fifth step is the design of the steel links. This requires the definition of the link length l_{link} from which the lever arm of the side steel columns is computed, i.e., $L_c = l_w + 2l_{link}$. Afterwards, the demand in terms of shear forces and bending moments in the links are derived following a uniform distribution among the links:

$$V_{link,Ed} = \frac{1}{n_{links}} CR \frac{M_{tot,Ed}}{L_c} \tag{8}$$

$$M_{link,Ed} = V_{link,Ed} l_{link} = \frac{l_{link}}{n_{links}} CR \frac{M_{tot,Ed}}{L_c} \tag{9}$$

The above formulas can be easily extended to the case of non-uniform link distributions, as illustrated in [12]. However, attention of this work is solely focused on uniform link distributions over the height of the building. Once the shear force and bending moment in the links are determined, their cross-section is selected accordingly.

The sixth step is the design of the steel side columns that must carry the summation of the shear forces in the links. Given that the side columns are non-dissipative elements, they are dimensioned according to capacity design rules conforming Eurocode 8 [26] recommendations for steel structures, i.e., the design axial force:

Table 3
Designed steel corner components.

Label	L_s (cm)	$N_{s,Ed}$ (kN)	Corner component diameter d_{cc} (mm)	Corner component thickness t_{cc} (mm)	Ω_{cc}
S3W75CR40-CCD	121	1313.97	95.0	16.0	1.06
S3W75CR50-CCD		1060.58		12.5	1.07
S3W75CR60-CCD		874.14		10.0	1.08
S3W75CR40-CCND	117	2035.13	133.0	16.0	1.05
S3W75CR50-CCND		1642.67		12.5	1.05
S3W75CR60-CCND		1353.90		10.0	1.04
S3W100CR40-CCD	82	1942.49	127.0	16.0	1.04
S3W100CR50-CCD		1553.67		12.5	1.05
S3W100CR60-CCD		1274.20		10.0	1.05
S3W100CR40-CCND	76	3170.70	193.7	16.0	1.05
S3W100CR50-CCND		2536.03		12.5	1.05
S3W100CR60-CCND		2079.86		10.0	1.04
S6W75CR40-CCD	259	1612.91	108.0	16.0	1.02
S6W75CR50-CCD		1305.56		12.5	1.02
S6W75CR60-CCD		1076.65		10.0	1.02
S6W75CR40-CCND	254	2467.93	159.0	16.0	1.07
S6W75CR50-CCND		1997.64		12.5	1.06
S6W75CR60-CCND		1647.38		10.0	1.05
S6W100CR40-CCD	186	2192.12	139.7	16.0	1.03
S6W100CR50-CCD		1787.88		12.5	1.02
S6W100CR60-CCD		1489.01		10.0	1.00
S6W100CR40-CCND	178	3434.78	219.1	16.0	1.12
S6W100CR50-CCND		2801.39		12.5	1.09
S6W100CR60-CCND		2333.09		10.0	1.06
S9W75CR40-CCD	397	2045.88	133.0	16.0	1.04
S9W75CR50-CCD		1659.52		12.5	1.04
S9W75CR60-CCD		1373.67		10.0	1.02
S9W75CR40-CCND	391	3116.50	193.7	16.0	1.07
S9W75CR50-CCND		2527.97		12.5	1.05
S9W75CR60-CCND		2092.52		10.0	1.03
S9W100CR40-CCD	287	2905.09	177.8	16.0	1.04
S9W100CR50-CCD		2301.84		12.5	1.05
S9W100CR60-CCD		1902.61		10.0	1.03
S9W100CR40-CCND	278	4507.02	273.0	16.0	1.09
S9W100CR50-CCND		3571.12		12.5	1.09
S9W100CR60-CCND		2951.75		10.0	1.06

$$N_{c,Ed} = 1.1\gamma_{ov}\sum_{i=1}^{n_{links}} V_{link,i} \tag{10}$$

is obtained amplifying N_c according to the factor $1.1\gamma_{ov}$ with $\gamma_{ov} = 1.25$. The effect of the eccentricity between the axis of the column and the connection transferring the shear force between the link and the column must be considered in the design.

The seventh and last step is the design of the transverse steel bars in the RC wall to provide adequate shear strength $V_{w,Rd}$. Allowance against non-ductile shear failure of the RC wall must be granted assuming that the entire base shear is resisted by the wall alone (the contribution of the two side columns is small and ignored in this design procedure). Accordingly, the base shear force $V_{pl,Ed}$ corresponding to the fully developed plastic mechanism (Fig. 2c) is derived from the rotational equilibrium with respect to the resultant of the lateral force distribution at an assumed height $H/2$ (an assumption that provided sufficiently accurate predictions of the numerical results as shown in [12]):

$$V_{pl,Ed} = \frac{M_{w,Rd} + M_{c,Rd}}{H/2} \tag{11}$$

where $M_{c,Rd} = 1.1\gamma_{ov}\ M_{c,Ed}$ is the bending resistance provided by the adopted side steel columns. In the case of RC wall with hinged base and corner components, given that the length of the wall must be reduced in the bottom part, i.e., the reduced length is $l_{w,red} < l_w$, attention should be given to the verification of the shear resistance of the reduced section.

2.3. Remarks on the design procedures

It is important to observe that the proposed design procedure, albeit apparently similar to the earlier formulation from which it is derived [12], exploits the role of CR in a very different way as compared to the previous studies [12–14]. In fact, in the current formulation the design solutions with different CR for a given building height are dimensioned to provide the same lateral capacity, i.e., the design total bending moment at the base is the same regardless of the adopted CR. On the other hand, in the mentioned previous parametric applications, the RC wall was the same for a given building height and the increment of CR was obtained increasing the contribution of the side columns. Accordingly, incrementing CR was also incrementing the lateral capacity of the designed SP-HCWs. Hence, the current study provides a different insight into the implications of the choice of CR in the design of SP-HCWs, allowing a clearer evaluation of its role now uncoupled from the increment of lateral capacity.

3. Numerical applications

3.1. Parametric analysis and case studies

The considered case studies consist of buildings with the same rectangular floor (25 m × 14 m), declined in three building heights, i.e., three-storey (H = 10.50 m), six-storey (H = 21.00 m), and nine-storey (H = 30.50 m), with constant 3.50 m inter-storey height from the ground to the last floor. Two SP-HCWs for each direction are the only structural elements providing lateral resistance against horizontal actions to a gravity-resistant steel frame (pinned base restraints as well as hinged beam-to-columns joints). Details on the architectural configuration and structural design of the gravity frame according to Eurocode 3 [29] can be found in [11]. The same geometry of previous works [11,12,14] on SP-HCWs was kept to allow comparisons with past results. For each considered building height, three design options at the base of the RC wall, i.e., fixed base and hinged base with corner components (either dissipative design or non-dissipative design), three values of CR (0.40,

Table 4
Designed steel links and side columns.

Label	$V_{link,Ed}$ (kN)	$M_{link,Ed}$ (kNm)	l_{link} (mm)	Link section	Ω_{link}	$N_{s,Ed}$ (kN)	L_c (mm)	Column section	Ω_{column}
S3W75CR40	167.55	41.89	250.0	HE140B	1.10	757.53	2.10	HE160M	1.23
S3W75CR50	202.86	48.69	240.0	HE160B	1.19	994.26	2.10	HE180M	1.18
S3W75CR60	250.79	57.68	230.0	HE180B	1.15	1192.94	2.10	HE200M	1.22
S3W100CR40	203.01	50.75	250.0	HE160B	1.19	994.26	1.75	HE180M	1.18
S3W100CR50	243.56	58.45	240.0	HE180B	1.19	1192.94	1.75	HE200M	1.22
S3W100CR60	299.62	68.91	230.0	HE200B	1.14	1407.69	1.75	HE220M	1.23
S6W75CR40	132.72	30.53	230.0	HE120B	1.09	1198.01	3.50	HE200M	1.21
S6W75CR50	161.14	34.65	215.0	HE140B	1.14	1515.06	3.50	HE220M	1.14
S6W75CR60	199.33	40.86	205.0	HE160B	1.21	1988.52	3.50	HE240M	1.20
S6W100CR40	161.83	37.22	230.0	HE140B	1.13	1515.06	2.80	HE220M	1.14
S6W100CR50	197.98	42.56	215.0	HE160B	1.22	1988.52	2.80	HE240M	1.20
S6W100CR60	247.32	50.70	205.0	HE180B	1.17	2385.88	2.80	HE260M	1.13
S9W75CR40	122.69	23.92	195.0	HE120B	1.18	1797.02	4.90	HE240M	1.33
S9W75CR50	149.28	26.87	180.0	HE140B	1.23	2272.59	4.90	HE280M	1.34
S9W75CR60	185.35	31.60	170.5	HE160B	1.30	2982.77	4.90	HE300M	1.30
S9W100CR40	160.54	31.31	195.0	HE140B	1.14	2272.59	3.85	HE280M	1.34
S9W100CR50	190.80	34.34	180.0	HE160B	1.26	2982.77	3.85	HE300M	1.30
S9W100CR60	236.57	40.33	170.5	HE180B	1.22	3578.82	3.85	HE320M	1.13

0.50, and 0.60), and two values for the ratio H/l_w (7.5 and 10.0), were considered. These assumptions lead to 54 case studies as listed in Table 1.

3.2. Seismic design

Regarding the design seismic input, the same total base moments obtained in [14] were used, i.e., 2567 kNm, 6587 kNm, and 13193 kNm for the three-storey, six-storey, and nine-storey cases, respectively, following Ground Type A of Eurocode 8 with design peak ground acceleration (PGA) $a_g = 0.20$ g, tentative behaviour factor q = 2, mass assigned to the SP-HCW of 158 kNs^2/m at floor levels and 132 kNs^2/m at roof level. Steel S355 (nominal yield stress $f_y = 355$ MPa) was adopted for the steel links, side columns, and corner components. Concrete C30 (characteristic compressive strength $f_{ck} = 30$ MPa) and steel reinforcements B450C (characteristic yield stress $f_{yk} = 450$ MPa) were used for the RC wall.

Table 2 reports the details of the design of the geometry and bending capacity of the RC walls for the 18 case studies with fixed base. The arrangement of the longitudinal rebars was made according to the rules for ductility class medium (DCM) of Eurocode 8 [26], i.e., the wall cross section is subdivided in side areas with more effective confining from stirrups and a central area that is defined as non-confined. The cross section of the three-storey case is an exception, resulting in a fully confined cross section due to the overlap of the side confined areas because of its smaller dimensions. The same geometry and longitudinal rebars were adopted for the case studies with hinged base, e.g., S3W75CR40, S3W75CR40-CCD, and S3W75CR40-CCND have the same RC wall apart from the base restraint and presence of corner components. Specifically, the data given in Table 2 are the wall length l_w and the wall width b_w (in the case of hinged base these two measures refer to the section above the reduction necessary for the corner components), the demand in term of bending moment in the wall $M_{w,Ed}$ as derived using Eq. (4), the adopted rebars and subsequent geometric ratio, i.e., area of the cross section of the rebars divided by the area of the concrete section, and the overstrength of the wall computed as $\Omega_{wall,M} = M_{w,Rd} / M_{w,Ed}$ being $M_{w,Rd}$ the capacity in bending as derived from conventional nonlinear sectional analysis according to Eurocode 2 [30] with partial safety factors of concrete and steel set to one. The values of $\Omega_{wall,M}$ are equal or slightly larger than the overstrength (1.50) enforced in the design procedure as previously described.

Table 3 gives the results of the design of the corner components selected in the European section catalogue of hollow circular sections being compact Class 1 according to Eurocode 3 [29]. The listed data are the following: the lever arm of the corner components L_s, the design axial force in the corner components $N_{s,Ed}$ computed using Eq. (6) in the case of dissipative design and Eq. (7) in the case of non-dissipative design, the external diameter d_{cc} and thickness t_{cc} of the selected cross section, and the overstrength factor of the corner components with respect to the design demand, computed as $\Omega_{cc} = N_{b,Rd} / N_{s,Ed}$.

Table 4 provides the outcomes of the design of the steel links. The demand in terms of shear and bending is determined through Eqs. (8) and (9). Afterwards, the design is based on the link properties and classification defined according to Eurocode 8 paragraph 6.8.2 [26], i.e., the link design yielding shear and bending are:

$$V_{p,link} = \frac{f_y}{\sqrt{3}} t_w (d - t_f) \tag{12}$$

$$M_{p,link} = f_y b t_f (d - t_f) \tag{13}$$

where d is section height, b is the flange width, t_f is the flange thickness, t_w is the web thickness. The adopted links are classified as short links according to Eurocode 8 given that the following relation $l_{link} < e_S$ where $e_S = 0.8 M_{p,link} / V_{p,link}$ holds for all cases. Links are the same for the case studies with the same RC wall, e.g., equal links for S3W75CR40, S3W75CR40-CCD, and S3W75CR40-CCND, hence, only labels referring to the 18 fixed base cases are listed. The overstrength of the links was computed considering the capacity and demand in shear, $\Omega_{link} = V_{p,link} / V_{link,Ed}$, being all short links.

Table 4 also lists the results of the design of the side columns. Specifically, the reported data are the design axial force obtained from Eq. (10), the adopted cross section taken among the European catalogue of wide-flange I-sections (HE sections), and the resulting overstrength Ω_{column} computed as the ratio between the nominal value of the yield strength and the stress due to axial force and bending due to the eccentricity of the axial force, including the effect of in-plane and out-of-plane instability according to Eurocode 3 [29]. All adopted cross sections are compact Class 1 according to Eurocode 3 [29]. As already commented for the design of the links, columns are the same for the case studies with the same RC wall, e.g., equal columns for S3W75CR40, S3W75CR40-CCD, and S3W75CR40-CCND, hence, only labels referring to the 18 fixed base cases are listed.

Table 5 provides the outcomes of the design of the shear reinforcement of the RC wall. The provided data are the reduced length of the wall at the base of the hinged designs to allow space to allocate the corner components, the design horizontal shear force as predicted using Eq. (11), the geometry of the stirrups (either single or double), their diameter (set to 10 mm for all cases), and their spacing (minimum admitted value 50 mm), the resulting overstrength in shear force,

Table 5
Designed RC walls (shear).

Label	$l_{w,red}$ (cm)	$V_{pl,Ed}$ (kN)	Stirrups: geometry / diameter (mm) / spacing (mm)	$\Omega_{wall,V}$
S3W75CR40	-	755.39	Single / ϕ10 / 100	1.14
S3W75CR50	-	762.85	Single / ϕ10 / 100	1.13
S3W75CR60	-	778.13	Single / ϕ10 / 100	1.11
S3W75CR40-CCD	101	621.67	Single / ϕ10 / 80	1.12
S3W75CR50-CCD	101	658.73	Single / ϕ10 / 75	1.13
S3W75CR60-CCD	101	692.94	Single / ϕ10 / 70	1.15
S3W75CR40-CCND	93	777.39	Single / ϕ10 / 70	1.09
S3W75CR50-CCND	93	780.17	Single / ϕ10 / 70	1.09
S3W75CR60-CCND	93	789.94	Single / ϕ10 / 70	1.07
S3W100CR40	-	788.18	Single / ϕ10 / 75	1.09
S3W100CR50	-	762.98	Single / ϕ10 / 75	1.12
S3W100CR60	-	768.85	Single / ϕ10 / 75	1.11
S3W100CR40-CCD	60	805.46	Double / ϕ10 / 90	1.13
S3W100CR50-CCD	60	853.36	Double / ϕ10 / 90	1.12
S3W100CR60-CCD	60	900.13	Double / ϕ10 / 90	1.08
S3W100CR40-CCND	46	811.09	Double / ϕ10 / 70	1.04
S3W100CR50-CCND	46	780.12	Double / ϕ10 / 70	1.08
S3W100CR60-CCND	46	779.64	Double / ϕ10 / 70	1.08
S6W75CR40	-	996.58	Single / ϕ10 / 160	1.10
S6W75CR50	-	988.45	Single / ϕ10 / 160	1.11
S6W75CR60	-	1061.51	Single / ϕ10 / 150	1.10
S6W75CR40-CCD	238	804.95	Single / ϕ10 / 150	1.09
S6W75CR50-CCD	238	834.97	Single / ϕ10 / 140	1.13
S6W75CR60-CCD	238	934.30	Single / ϕ10 / 130	1.09
S6W75CR40-CCND	228	1039.62	Single / ϕ10 / 130	1.07
S6W75CR50-CCND	228	1018.20	Single / ϕ10 / 130	1.10
S6W75CR60-CCND	228	1080.80	Single / ϕ10 / 120	1.12
S6W100CR40	-	986.59	Single / ϕ10 / 120	1.11
S6W100CR50	-	1005.41	Single / ϕ10 / 120	1.09
S6W100CR60	-	1031.95	Single / ϕ10 / 120	1.06
S6W100CR40-CCD	162	805.46	Single / ϕ10 / 100	1.11
S6W100CR50-CCD	162	853.36	Single / ϕ10 / 95	1.11
S6W100CR60-CCD	162	900.13	Single / ϕ10 / 90	1.11
S6W100CR40-CCND	146	1053.75	Single / ϕ10 / 80	1.10
S6W100CR50-CCND	146	1047.00	Single / ϕ10 / 80	1.11
S6W100CR60-CCND	146	1054.84	Single / ϕ10 / 80	1.10
S9W75CR40	-	1332.03	Single / ϕ10 /180	1.10
S9W75CR50	-	1334.01	Single / ϕ10 / 180	1.10
S9W75CR60	-	1446.96	Single / ϕ10 / 170	1.08
S9W75CR40-CCD	373	1096.60	Single / ϕ10 /170	1.11
S9W75CR50-CCD	373	1140.40	Single / ϕ10 / 160	1.13
S9W75CR60-CCD	373	1282.37	Single / ϕ10 / 150	1.07
S9W75CR40-CCND	361	1384.90	Single / ϕ10 /150	1.11
S9W75CR50-CCND	361	1365.53	Single / ϕ10 / 150	1.12
S9W75CR60-CCND	361	1462.40	Single / ϕ10 / 140	1.12
S9W100CR40	-	1350.19	Single / ϕ10 / 130	1.13
S9W100CR50	-	1358.77	Single / ϕ10 / 130	1.12
S9W100CR60	-	1395.27	Single / ϕ10 / 130	1.09
S9W100CR40-CCD	259	1105.56	Single / ϕ10 / 120	1.08
S9W100CR50-CCD	259	1168.63	Single / ϕ10 / 110	1.12
S9W100CR60-CCD	259	1134.82	Single / ϕ10 / 110	1.15
S9W100CR40-CCND	240	1418.58	Single / ϕ10 /100	1.08
S9W100CR50-CCND	240	1412.89	Single / ϕ10 / 100	1.08
S9W100CR60-CCND	240	1330.07	Single / ϕ10 / 100	1.15

determined as the ratio $\Omega_{wall,V} = V_{s,Rd} / V_{pl,Ed}$, with $V_{s,Rd}$ evaluated according to Eurocode 2 [30] using partial safety factors for concrete and steel rebars set to one.

3.3. Finite element model

A two-dimensional nonlinear finite element model as depicted in Fig. 4 is implemented in the software OpenSees [31], following the same approach detailed in [14]. Geometric nonlinearity is included in the model using a Corotational coordinates transformation. Such nonlinear finite element model was validated thorough comparisons with experimental tests available in the technical literature for steel links and RC walls with similar geometries, as detailed in [14].

The elastic axial and flexural behaviour of the steel link is modelled with an Euler-Bernoulli beam element while the plastic flexural response and the elastoplastic shear response are lumped at the link end connected to the RC wall, using zero-length elements with an uniaxial nonlinear elastoplastic constitutive law [32], previously implemented in OpenSees with the name SteelBRB [33]. A similar model with the same elastoplastic constitutive law was successfully adopted and validated against experimental results in [34] for dissipative links in eccentrically braced frames. An example of shear versus rotation monotonic response in shown in Fig. 5a for a link with section HE160B.

A couple of truss elements, transmitting axial force only, are used to model the corner components; their nonlinear behaviour is described using the nonlinear elastoplastic constitutive law Steel02 available in OpenSees. An example of axial force versus axial strain monotonic response in shown in Fig. 5b for a corner component with section having diameter 139.7 mm and thickness 12.5 mm.

A force-based distributed-plasticity fibre frame element is used to

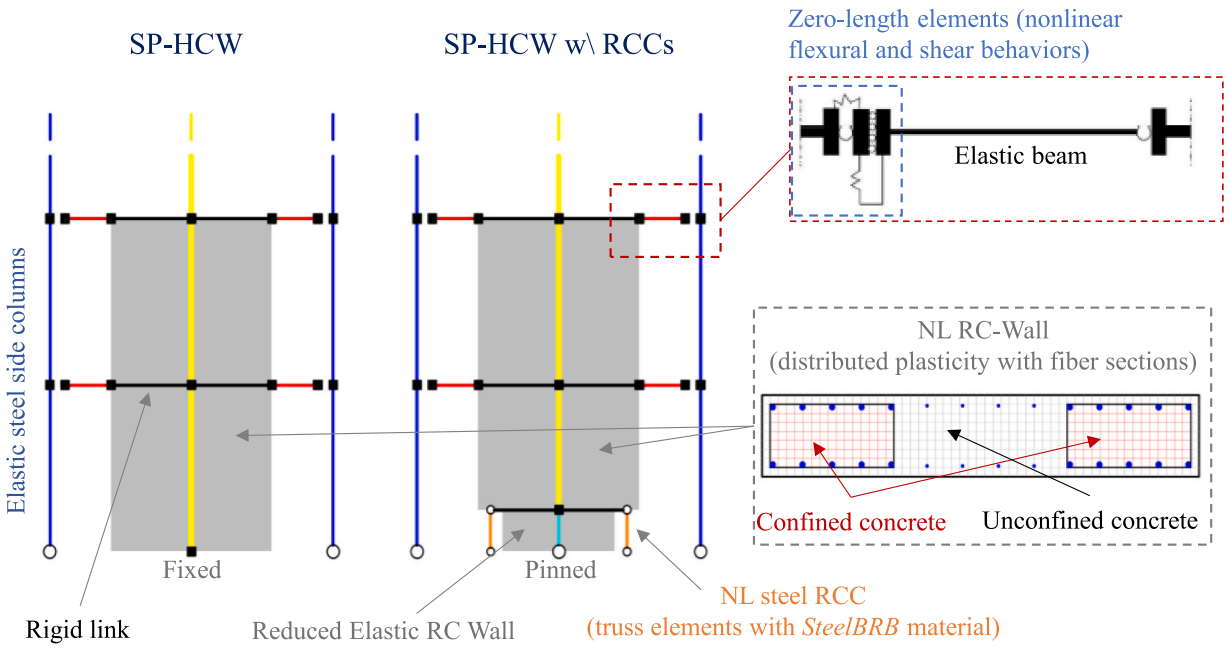

Fig. 4. Finite element models.

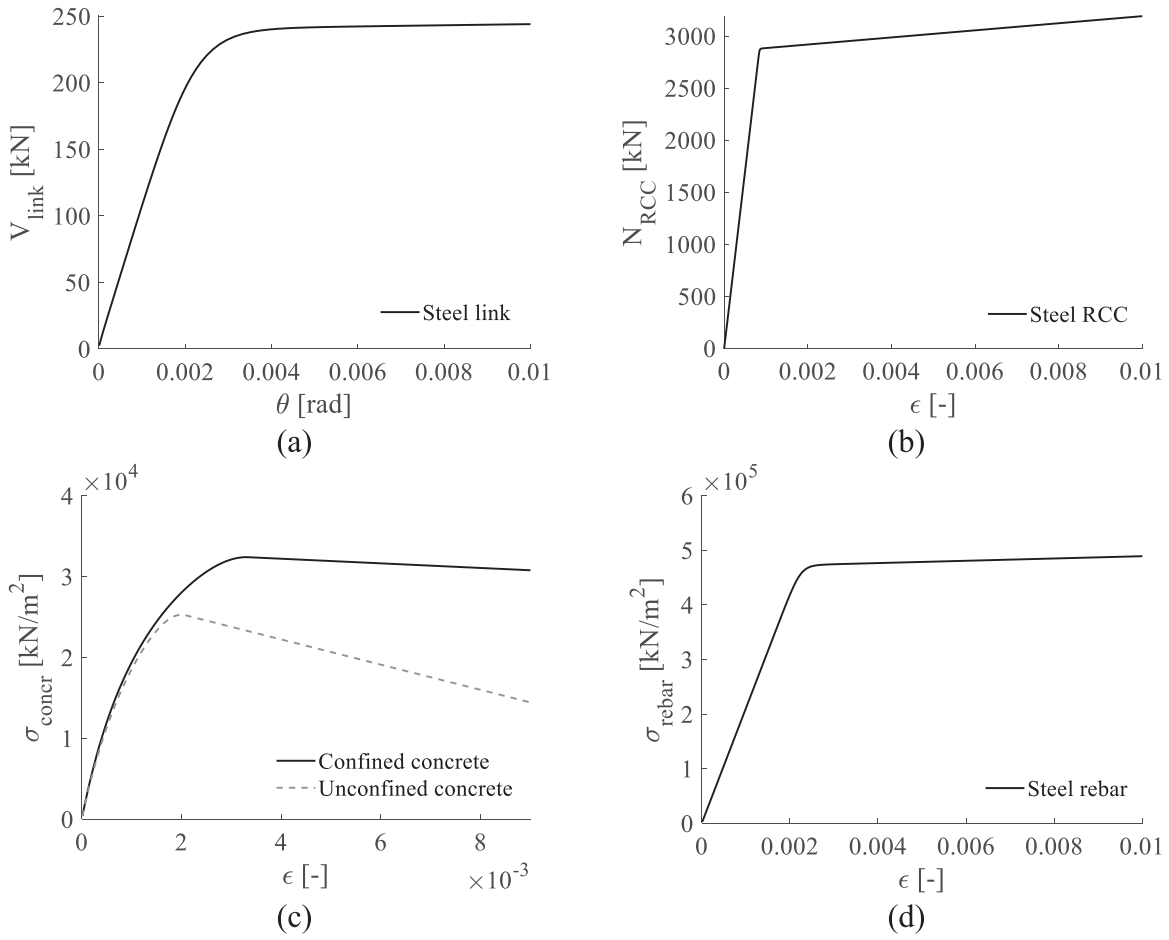

Fig. 5. Materials constitutive laws: (a) steel links; (b) steel RCCs; (c) confined and unconfined concrete; (d) steel rebars.

describe the flexural behaviour of the RC wall, with different constitutive laws (monotonic response in Fig. 5c) for the confined and unconfined portions of the concrete cross section. The shear behaviour of the RC wall elements is modelled as linear elastic. Steel rebars have perfect bond with the surrounding concrete and are modelled with the Steel02 constitutive law (monotonic response in Fig. 5d).

Table 6
RC-Wall shear demand/capacity ratios.

Label	V_{Ed}/V_{Rd}	Label	V_{Ed}/V_{Rd}
S3W75CR40	0.53	S6W100CR40	0.61
S3W75CR50	0.50	S6W100CR50	0.59
S3W75CR60	0.47	S6W100CR60	0.59
S3W75CR40-CCD	0.48	S6W100CR40-CCD	0.58
S3W75CR50-CCD	0.44	S6W100CR50-CCD	0.54
S3W75CR60-CCD	0.41	S6W100CR60-CCD	0.51
S3W75CR40-CCND	0.51	S6W100CR40-CCND	0.55
S3W75CR50-CCND	0.48	S6W100CR50-CCND	0.53
S3W75CR60-CCND	0.47	S6W100CR60-CCND	0.53
S3W100CR40	0.54	S9W75CR40	0.62
S3W100CR50	0.50	S9W75CR50	0.60
S3W100CR60	0.48	S9W75CR60	0.55
S3W100CR40-CCD	0.37	S9W75CR40-CCD	0.58
S3W100CR50-CCD	0.35	S9W75CR50-CCD	0.53
S3W100CR60-CCD	0.33	S9W75CR60-CCD	0.48
S3W100CR40-CCND	0.51	S9W75CR40-CCND	0.57
S3W100CR50-CCND	0.49	S9W75CR50-CCND	0.57
S3W100CR60-CCND	0.48	S9W75CR60-CCND	0.53
S6W75CR40	0.61	S9W100CR40	0.60
S6W75CR50	0.59	S9W100CR50	0.58
S6W75CR60	0.55	S9W100CR60	0.57
S6W75CR40-CCD	0.59	S9W100CR40-CCD	0.59
S6W75CR50-CCD	0.54	S9W100CR50-CCD	0.52
S6W75CR60-CCD	0.50	S9W100CR60-CCD	0.51
S6W75CR40-CCND	0.58	S9W100CR40-CCND	0.57
S6W75CR50-CCND	0.55	S9W100CR50-CCND	0.57
S6W75CR60-CCND	0.50	S9W100CR60-CCND	0.56

3.4. Seismic performance evaluation

The seismic performance is evaluated according to paragraph 4.3.3.4.2 of Eurocode 8 [26], i.e., through nonlinear static (pushover analysis). The objectives of this evaluation are: 1) assessment of the results obtained with the proposed design approach; 2) insight into the resisting mechanisms activated in the post-elastic response to understand their influence over the global seismic capacity of SP-HCWs.

The main events are marked directly in the figures, i.e., first steel link yielding, yielding of all the steel links, first yielding of the rebars in the RC wall, yielding of the corner components, strains - 0.0035 (at stress peak) and - 0.0088 (ultimate) in the concrete (according to the adopted confined concrete model and here used as indicators of damage of concrete in compression), ultimate rotation in the steel links according to Eurocode 8 [26]. Other two critical conditions, i.e., the attainment of the steel side column capacity according to Eurocode 3 [29] and the attainment of the shear capacity of the RC wall according to Eurocode 2 [30], are not directly included in the model and are verified in post-processing. The relevant markers are not present in the figures as such critical conditions were never reached during the performed analyses.

The maximum base shear force in each pushover curve is always smaller than the values of the shear capacity in Table 5, as reported in Table 6. Hence, the overstrength in shear resistance assigned to the SP-HCWs by the proposed design procedure is appropriate in avoiding failure in shear in the RC wall.

3.5. Seismic performance: influence of the base connection

Fig. 6 presents the pushover curves, i.e., base shear as a function of the roof drift ratio (RDR), i.e., the horizontal top displacement of a control point normalised by the building height H, for the designs with CR = 0.50 and $H/l_w = 10$ in the three-storey (Fig. 6a), six-storey (Fig. 6c), and nine-storey (Fig. 6e) cases. The relevant moment-curvature response in RC wall sections of the three-storey (Fig. 6b), six-storey (Fig. 6d), and nine-storey (Fig. 6f) cases are also reported. Results concern the base section for the fixed base cases and the lower section with unreduced dimension (just above the top end of the corner components) for the hinged case. Dimensions and rebars of the cross sections are the same for an assigned building height and CR, regardless the other design parameters, as already discussed in paragraph 3.2.

The design solutions with fixed base (S3W100CR50, S6W100CR50, and S9W100CR50) are presented for comparison and confirm the result observed in previous studies, i.e., yielding of all links is activated when the rebars in the RC wall are still in their elastic range, with the only exceptions of a reduced subset of systems with CR = 0.60 for which the first rebar yielding is attained simultaneously to (or slightly before) the complete activation of the links. However, some critical aspect are observed in the case of fixed base: i) in the three-storey case rebar yielding starts followed by the attainment of the peak of concrete stress and ultimate strain along the plastic plateau of the pushover curve, while the link rotation capacity is never reached, accordingly the plastic resources are not fully exploited; ii) in the six-storey case rebar yielding occurs earlier while concrete peak and ultimate strain are slightly postponed as compared to the three-storey cases, however, the link rotation capacity is reached just after the concrete peak strain; iii) in the nine-storey case the global behaviour is similar to the six-storey case with the difference that the link rotation capacity occurs when rebars start yielding. Consequently, the fixed base solutions do not provide a satisfying seismic performance because of the uniform distribution of links over the building height that requires a redistribution of forces not compatible with the link rotation capacity [12]. Further considerations on this issue are not in the objectives of this study that is focusing only on the use of the simpler uniform distribution of dissipative steel links.

The solutions with hinged base and non-dissipative design of the corner components (S3W100CR50-CCND, S6W100CR50-CCND, and S9W100CR50-CCND) show a global response very similar to the cases with fixed base. However, in this case damages in the RC wall are significantly postponed (both in rebars and concrete) and the ultimate concrete strain is never reached within the explored RDR range. This aspect is also shown in the moment-curvature responses in Fig. 6b,d,f where much lower curvatures are developed in the hinged base cases. On the other hand, minor benefits in terms of rotation demand in the steel link are obtained by the hinged design with non-dissipative corner components, especially in the nine-storey case.

The solutions with hinged base and dissipative design of the corner components (S3W100CR50-CCD, S6W100CR50-CCD, and S9W100CR50-CCD) have a different global behaviour due to the earlier yielding of the corner components as compared to solutions with hinged base and non-dissipative design of the corner components. The steel links and the corner components are involved in the plastic behaviour at the same time and the solution provides an optimal post-elastic response. The objective of further reducing damage in the RC wall is fully achieved, as testified by the fact that the peak strain in the concrete in not attained for the whole range of RDR. The dissipative design of the corner components is also beneficial in terms of reduction of the rotation demand in the steel links, as observed in Fig. 6c,e. However, these benefits are paid through a reduction of about 20 % of the horizontal force capacity of the SP-HCW.

It is worth noting that the nonlinear behaviour of the RC wall has an important impact on the response of the dissipative links. Because of the concrete nonlinearity, the neutral axis of the RC wall shifts towards its compressed side, resulting in an asymmetric behaviour (in terms of both shear forces and rotations demand) of the links in the tensioned side and those on the compressed side of the wall, as depicted in Fig. 7, where plots for the six-storey buildings with fixed base (S6W100CR50) and hinged base (S6W100CR50-CCND) are reported. More in detail, the evolution of the shear force (Fig. 7a-c) and rotation (Fig. 7b-d) of the links with RDR is represented using different colours for the links on the tensioned and compressed sides of the wall. It can be observed that the entity of the rotation demand (Fig. 7d) is notably lower on the links in the compressed side. The same behaviours are observed on the systems with three- and nine-storeys, as displayed in Fig. 8 for the case of hinged connection. Similar trends were observed in all the other case studies not

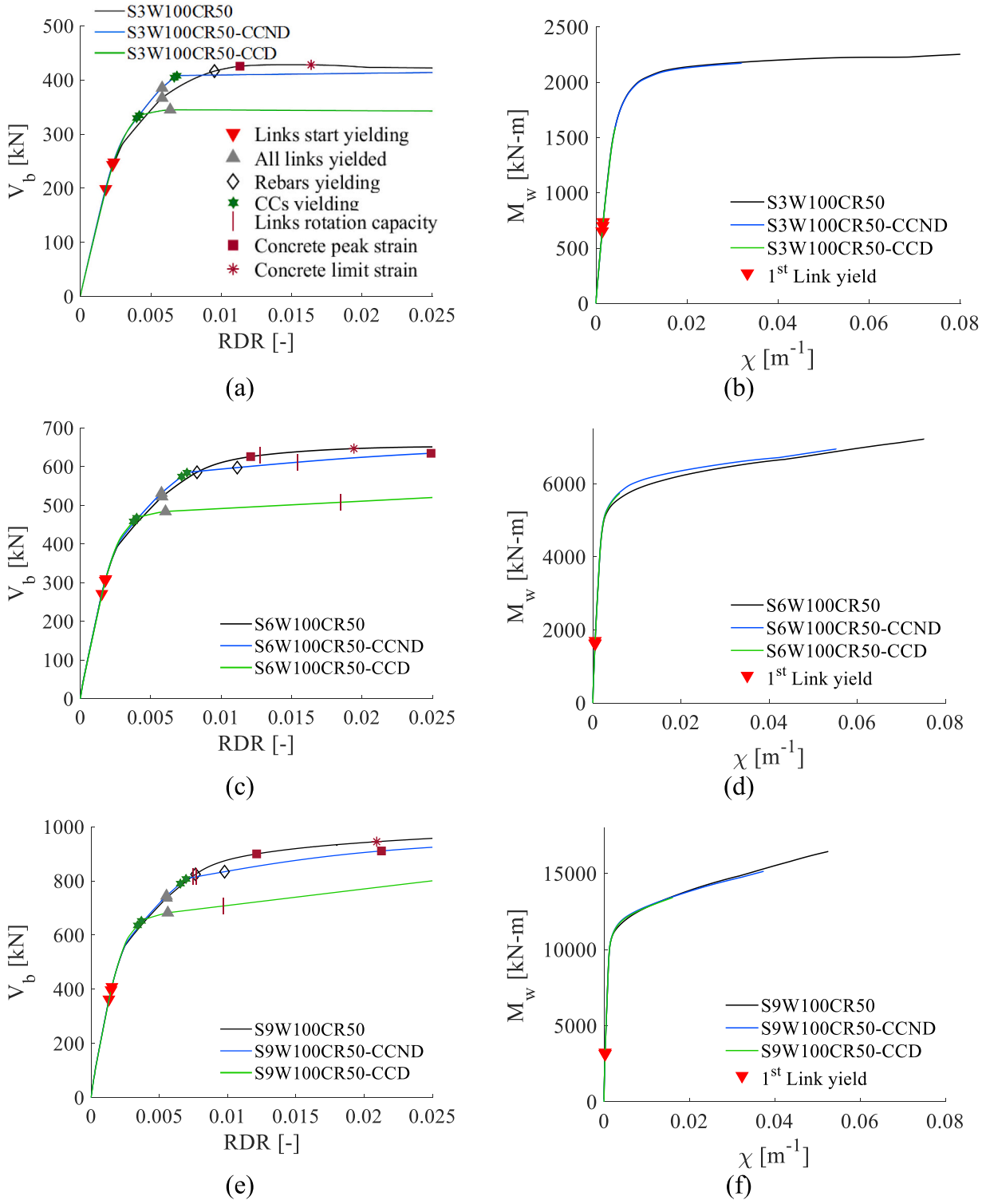

Fig. 6. Influence of the base connection: capacity curves (left-hand side) and moment-curvature response in the RC wall (right-hand side) for CR = 50 in the three-storey (a,b), six-storey (c,d), and nine-storey cases (e,f).

shown in the figures.

An additional comment can be made on the global response of the considered SP-HCW designs where it is noted that the event providing the largest reduction in lateral stiffness is the transition of the base of the RC wall from the elastic to the plastic range. Such a behaviour is particularly evident in the case of corner components given the sharper change of stiffness due to the lack of internal redistribution that instead occur in the RC. This observation confirms the fundamental role of the RC wall in providing lateral stiffness to the SP-HCW.

3.6. Seismic performance: influence of CR

Further insight on the seismic performance of SP-HCWs is provided in Fig. 9, Fig. 10, and Fig. 11 illustrating the pushover curves for the different design values of CR as well as the effective CR as computed from M_c and M_w obtained in the analysis, afterwards given in Fig. 12. It

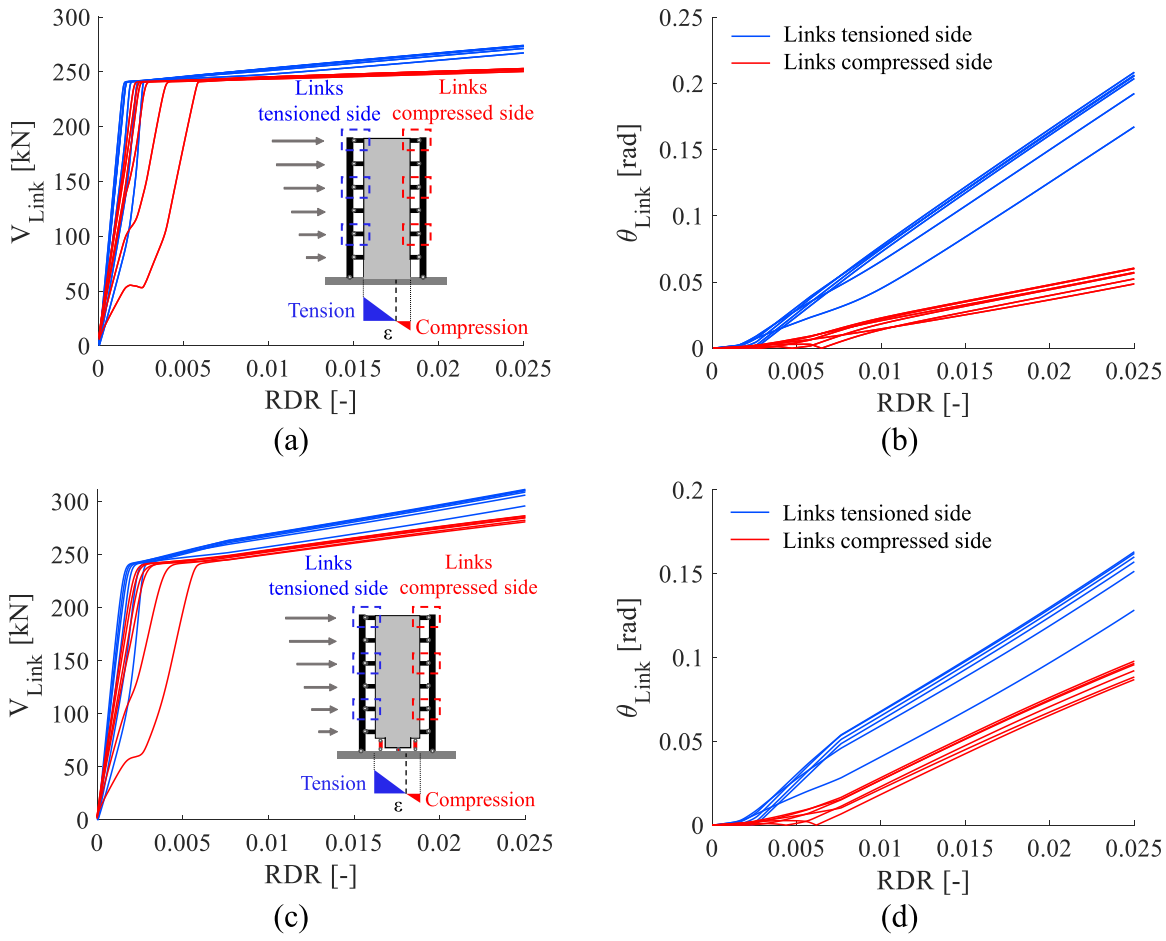

Fig. 7. Response comparison between links in the tensioned and compressed sides for the (a, b) S6W100CR50 and (c, d) S6W100CR50-CCND systems: (a, c) shear forces and (b, d) links rotation as a function of RDR.

is noted that: i) in the fixed base solutions a lower CR in the design has a small but noticeable effect in reducing the strain demand in the RC wall, as well as the rotations in the steel links; ii) in the hinged base designs the opposite effect is observed, even though the influence of the design CR is smaller; iii) the effective CR is closer to the design CR in the case of dissipative corner components as in this case no overstrength that modify the balance between the RC wall and the steel side columns is introduced. The plots of Fig. 12 testify the design equivalence achieved, for equal CR values, by different base connection strategies; the fixed and hinged base solutions provide very similar base bending moments, with the M_c curves perfectly superimposed and the M_w contributions provided by the non-dissipative RCCs closely matching those offered by the fixed-base wall. The values of M_w resisted by the hinged solutions with dissipative RCCs are lower compared to the other two base connection strategies (i.e., fixed or hinged with non-dissipative RCCs), consistently with the RC wall design objective without overstrength.

3.7. Seismic performance: influence of the RC wall geometry

Finally, Fig. 13 and Fig. 14 report the comparisons between the designs using RC walls with different slenderness ratio, $H/l_w = 10$ and $H/l_w = 7.5$. A horizontal shift of the pushover curves is observed due to the increased lateral stiffness when a larger RC wall is adopted (the critical events marked in the figure are attained at a slightly larger base shear but also at a lower value of RDR). While this observation might appear to indicate that designing a larger wall is not beneficial, it should be also noted that the solution with $H/l_w = 7.5$ allows reducing detailing problems due to crowded rebars both in flexure and shear, especially at the base of lower buildings where the corner components strongly reduce the resisting section of the bottom part of the RC wall.

3.8. Seismic performance: system ductility

The results of the pushover analysis can be processed to obtain measures of the ductility of the proposed SP-HCW system that quantify the previous comments based on the observation of the capacity curves. Focus is made on three conditions: i) yielding of all the steel links connecting the steel side columns to the RC wall; ii) first yielding of rebars in the RC wall; iii) failure either determined by the ultimate rotation capacity of the steel links or ultimate strain in the RC wall. For each case study three values were computed, i.e., the ratios between the lateral displacement of the top storey (roof level) when each of the three considered conditions is attained versus the lateral displacement of the same storey when the first link yielding occurs. The obtained results are indicated as μ_L, μ_D, μ_F for the conditions of all links yielded, first rebar yielded, and failure, respectively; their values are listed in Table 7 (fixed base), Table 8 (hinged base with non-dissipative corner components), and Table 9 (hinged base with dissipative corner components). The minimum value $min(\mu_D, \mu_F)$ between μ_D and μ_F is also reported as values of μ_D higher than μ_F cannot be physically achieved; they are obtained in the analysis because of the failure conditions are verified in the post-processing phase, as previously explained.

The condition $\mu_L < \mu_D$ allows to assess the achievement of no damage in the RC wall when the steel links are yielded. It is observed that μ_L increases with the number of building storeys and with CR; the base restraint has a limited yet non-negligible influence on μ_L with lower

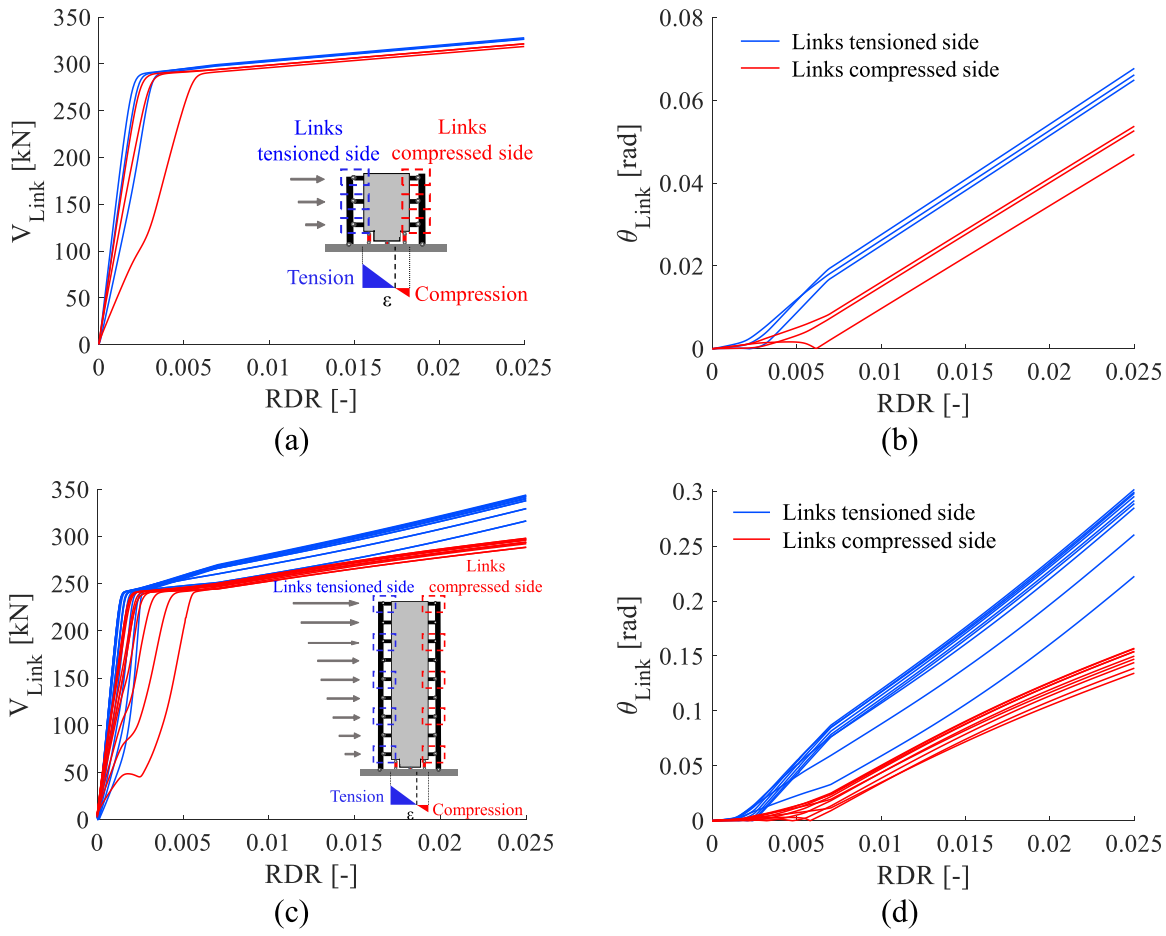

Fig. 8. Response comparison between links in the tensioned and compressed sides for the three- and nine-storey systems: (a, b) S3W100CR50-CCND and (c, d) S9W100CR50-CCND; (a, c) shear forces and (b, d) links rotation as a function of RDR.

values in the hinged base designs. On the other hand, it is noted that μ_D decreases with CR in the case of fixed base where its value is generally higher than μ_L with few exceptions. Therefore, the lower CR = 0.40 appears as a better design option as the complete yielding of links is anticipated (lower μ_L) while yielding in the rebars of the RC wall is postponed (higher μ_D). Much higher values of μ_D are obtained in the cases with hinged base, especially when dissipative corner components are used, making the fulfilment of the design objective of no damage in the RC wall much easier, as already commented in the analysis of the results in the previous sections. Regarding the attainment of the failure condition, it is observed that μ_F significantly reduces with the increment of the number of storeys, highlighting that the application of SP-HCWs to tall buildings cannot be conveniently made using a uniform link distribution over the height, as already commented. Nevertheless, the relation $\mu_L < \mu_F$ is always satisfied, hence, the condition of yielding of all links is achieved in all the designed case studies before attainment of failure.

Table 10 reports the mean values of μ_L and $min(\mu_D, \mu_F)$ as well as their coefficients of variation (COV), i.e., the ratio between the standard deviation and the mean value, computed for each base condition considering as input data, in turns, the ratios obtained from all the 18 designs, only the six designs with the same CR, and only the six designs with the same number of storeys. It is observed that μ_L for the fixed base designs ranges between 3.0 and 6.0 with an overall mean value of 3.9; such values reduce to the range 2.5 to 5.0 with mean value 3.5 in the hinged base with non-dissipative corner components, and 2.0 to 4.5 with mean value 3.3 in the hinged base with dissipative corner components. The dependency of μ_L on CR and number of storeys is evident in Table 10, i.e., systematic increment of μ_L when CR is increased and/or when the building height is increased. In the case of CR = 40 % the mean values of μ_L drop to 3.2, 2.9, and 2.7 for the fixed base, hinged base with non-dissipative corner components, and hinged base with dissipative corner components, respectively.

Regarding $min(\mu_D, \mu_F)$, the fixed base and the hinged base designs show very different values. In the fixed base the overall mean value of $min(\mu_D, \mu_F)$ is 5.1 while the mean values for CR = 40 %, 50 %, and 60 %, are 5.6, 5.3, and 4.5, respectively, denoting a decrement with the increment of CR. Much larger values are found in the hinged base designs, consistently with the comments made in the previous section on the outcomes of the nonlinear analyses. Such results indicate a ductile behaviour of the proposed SP-HCW solutions together with the inherent difficulties in defining a unique limit ductility factor that apply to all cases regardless of the building height and CR adopted in the design.

4. Conclusions

Hybrid coupled walls (HCWs) made of a single reinforced concrete (RC) wall connected to two steel side columns through steel links, named here as single-pier HCWs (SP-HCWs), were studied. The steel links are intended to work as elements dissipating seismic energy while the steel side columns and the RC wall should remain elastic. Previous studies highlighted the potentialities of SP-HCWs but also noted the occurrence of damage at the base of the RC wall that might not be easy and economical to repair. Accordingly, in this study specific attention was given to solutions able to reduce the damage at the base of the RC wall under lateral loads. To this end, the scheme of SP-HCW with fixed base, adopted in former investigations, was modified through the introduction of a hinged base together with vertical steel elements called

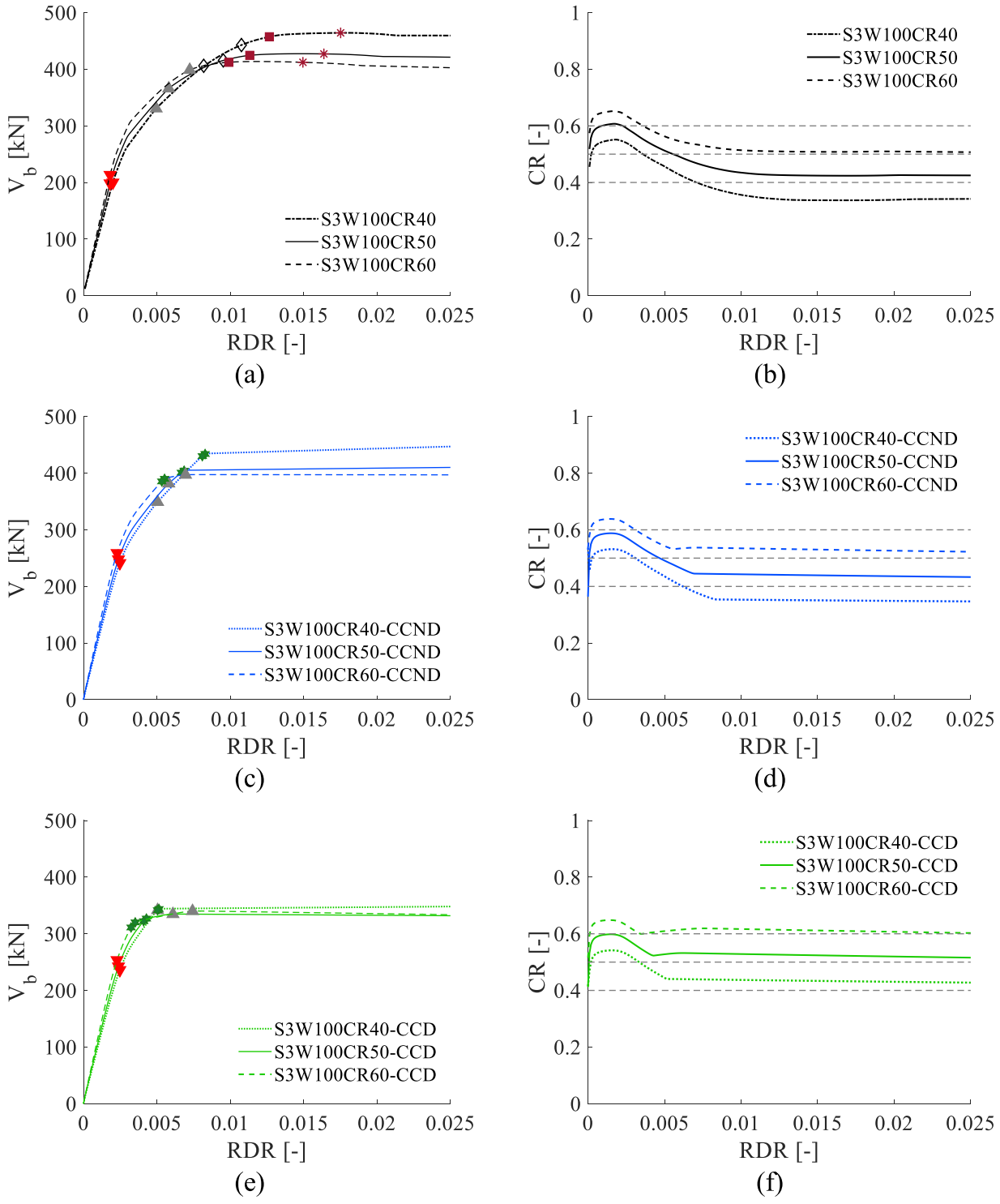

Fig. 9. Influence of CR: capacity curves (left-hand side) and evolution of the effective CR (right-hand side) in the three-storey for fixed base (a,b), hinged base with non-dissipative corner components (c,d) and dissipative corner components (e,f).

corner components.

A dedicated ductile design methodology that provides indications for dimensioning each component was presented and applied in a parametric analysis involving the design of 54 case studies with different building heights (three-, six-, and nine-storey), coupling ratios (0.40, 0.50, and 0.60), height-to-length ratio of the RC wall (7.5 and 10.0), in addition to different base conditions (fixed base, hinged base with corner components designed as non-dissipative elements, hinged base with corner components designed as dissipative elements). The proposed design procedure is at the same time an improvement for fixed base SP-HCWs of the previous design approach from which it is derived and an extension to the hinged base solution with corner components designed only to protect the RC wall or designed to also collaborate to the dissipative mechanism together with the steel links connecting the side columns to the RC wall.

The nonlinear finite element analyses of the considered case studies gave the following results:

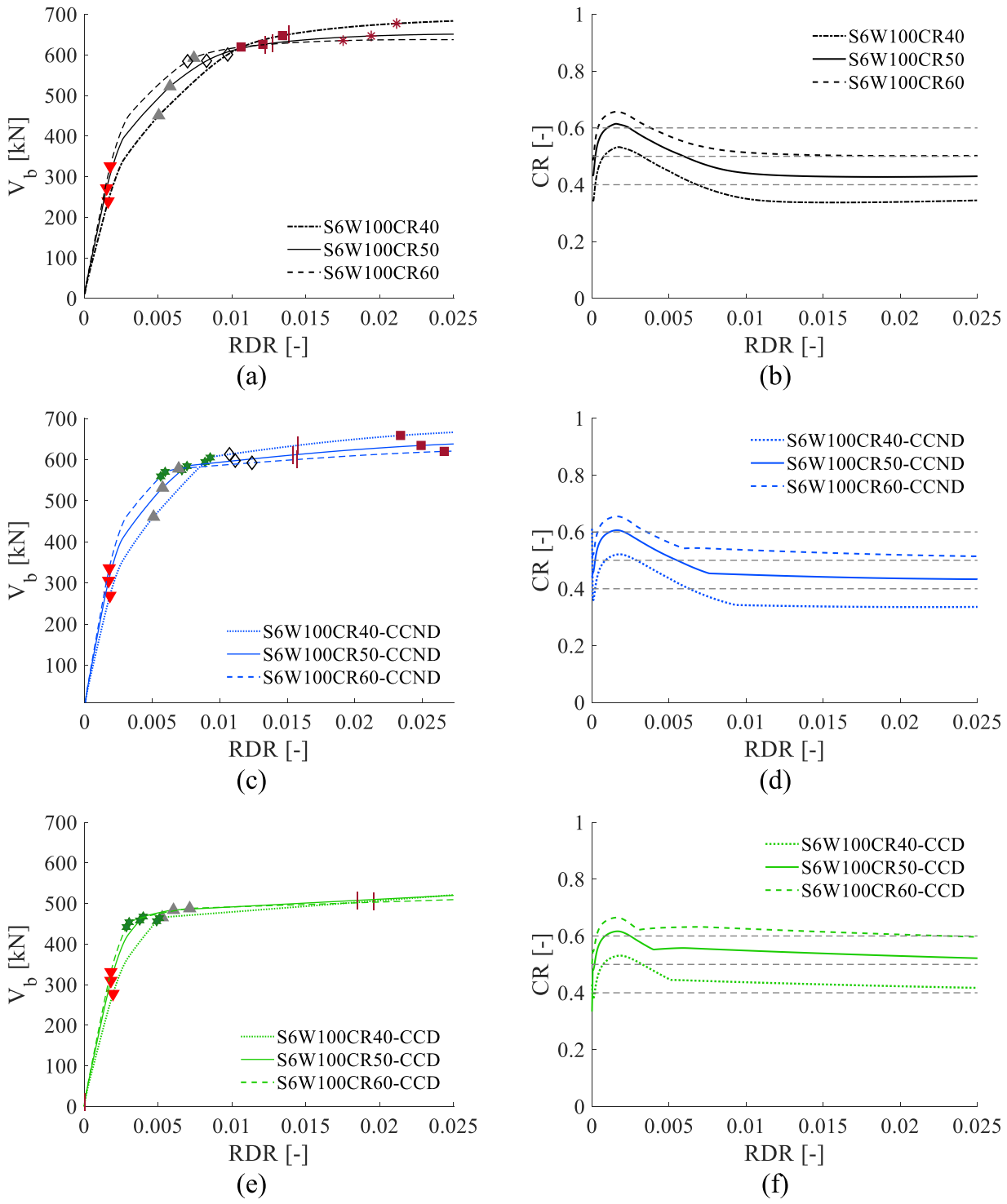

Fig. 10. Influence of CR: capacity curves (left-hand side) and evolution of the effective CR (right-hand side) in the six-storey for fixed base (a,b), hinged base with non-dissipative corner components (c,d) and dissipative corner components (e,f).

- The proposed design procedure provides ductile solutions where all the steel links (dissipative elements) yield when the rebars in the RC wall and the steel side columns are still in their elastic state (rebar yielding occurs slightly before the complete activation of the links in only 3 cases with fixed base and CR=0.60).
- The proposed solution with hinged base and corner components behaves notably better with respect to the solution with fixed base. In particular, the adoption of a hinged base with corner components significantly drops the strain demand in bending of the RC wall. The benefit is enhanced in the case of corner components designed as dissipative elements, yielding together with the steel links, even if this design option results in a reduction of the capacity to resist horizontal actions.
- The rotational demand in the steel links is a concern for six-storey buildings and becomes a major problem for the nine-storey buildings when a fixed base together with a uniform distribution of the links over the building height is used; the adoption of a hinged base is

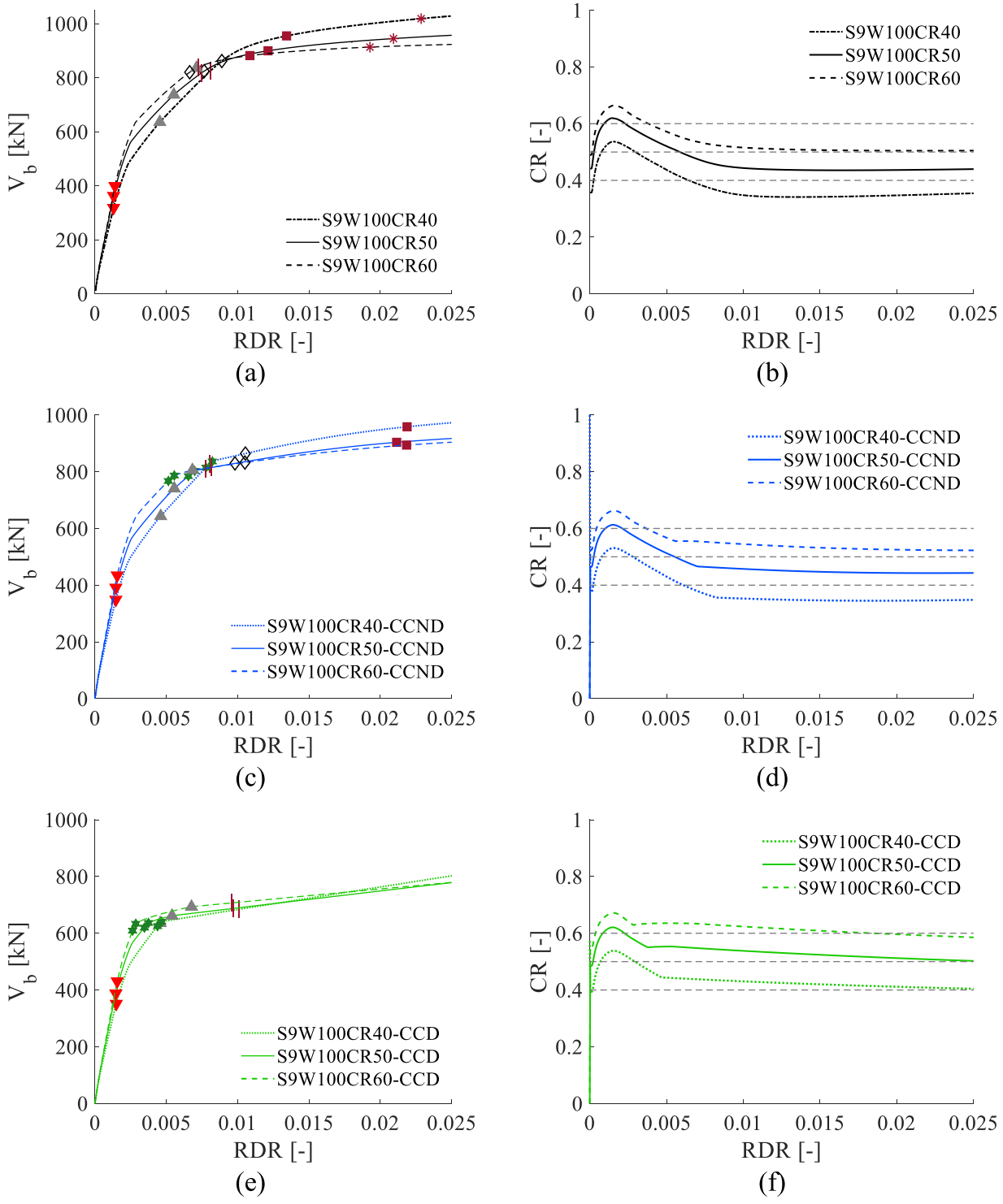

Fig. 11. Influence of CR: capacity curves (left-hand side) and evolution of the effective CR (right-hand side) in the nine-storey for fixed base (a,b), hinged base with non-dissipative corner components (c,d) and dissipative corner components (e,f).

beneficial in this aspect, especially in the case of corner components designed as dissipative elements.

- CR in the range between 0.40 and 0.60, where the steel side columns and the RC wall are designed to share similar portions of the total base moment, has a small yet non-negligible influence on the yielding of the steel links, on strain demand in the RC wall, and on the rotation demand in the steel links. Namely, the lower value of CR anticipates yielding of all steel links (for both fixed and hinged base designs) and lowers the strain and rotation demands in the case of fixed base while in the hinged base designs the opposite effect is observed to a smaller extent. Accordingly, given that in the hinged base designs the strain and rotation demands are less critical, the lower bound of CR appears as the preferred choice in the design of SP-HCWs.
- Using smaller values of the height-to-length ratio of the RC wall (7.5 instead of 10) showed little differences in terms of global behaviour. However, in this case there are significant benefits in the detailing of

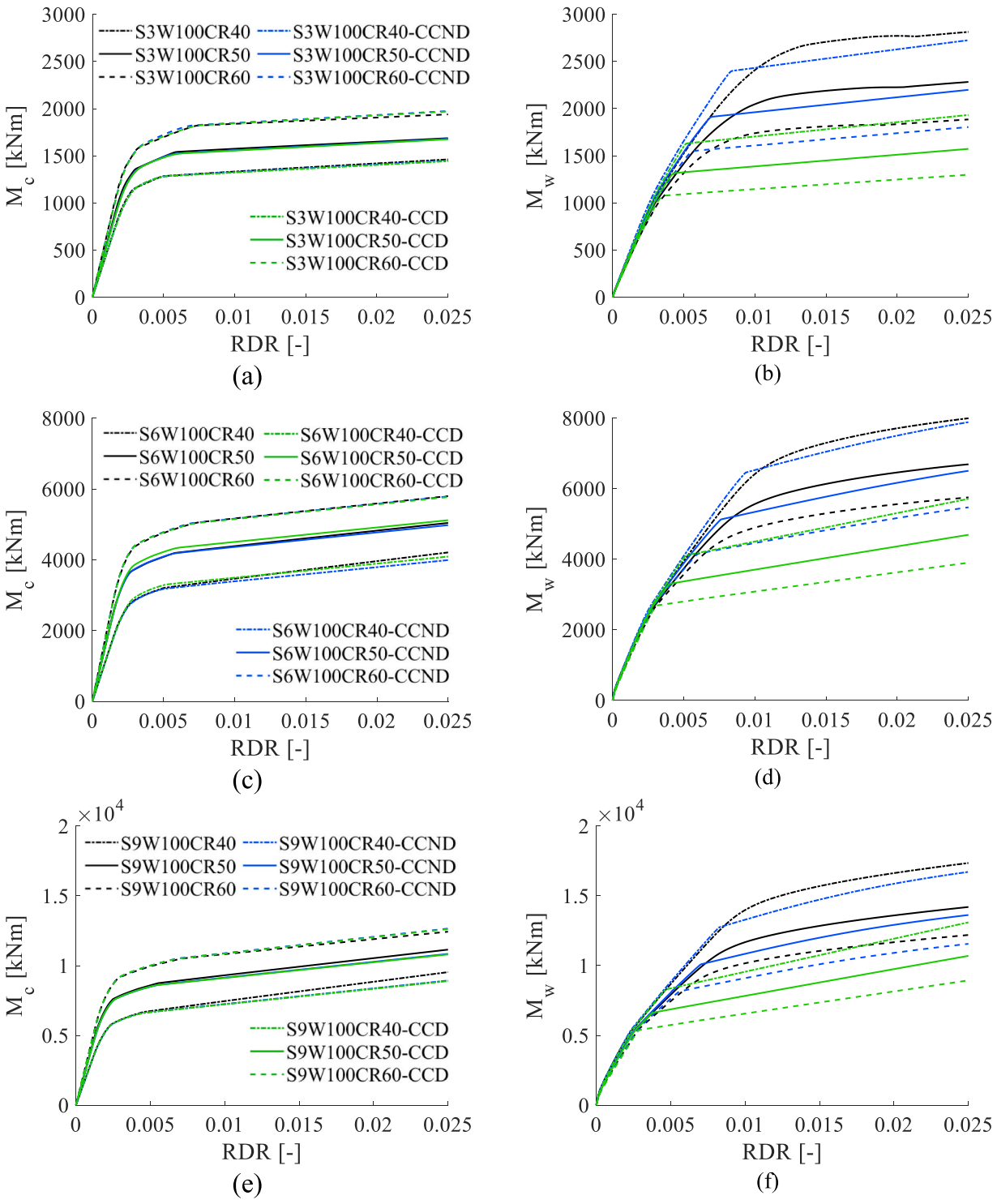

Fig. 12. Influence of CR: moment contributed by the side columns (left-hand side) and moment contributed by the RC wall (right-hand side) as functions of the RDR in the three-storey (a,b), six-storey (c,d), and nine-storey cases (e,f).

the RC wall as less crowded arrangements of longitudinal rebars and stirrups are obtained.

Based on the design developments and numerical results obtained in this work, it can be concluded that a hinged base with corner components in SP-HCWs is a viable possibility providing two kinds of benefits as compared to the fixed base condition: 1) increased protection of the RC wall from possible damages; 2) reduction of rotation demand in the steel links highlighted as a critical aspect, especially when the height of the building increases and a simple uniform link distribution over the building height is used. Such benefits are amplified when the corner components collaborate to the dissipative mechanisms together with the links connecting the side columns to the RC wall, i.e., the so-called dissipative design of the corner components. Further studies to consolidate these results should be foreseen, based on both numerical simulations of the nonlinear dynamic seismic response within a probabilistic framework aimed at analysing the seismic reliability of the proposed SP-HCWs and experimental testing, to fine-tune the proposed design

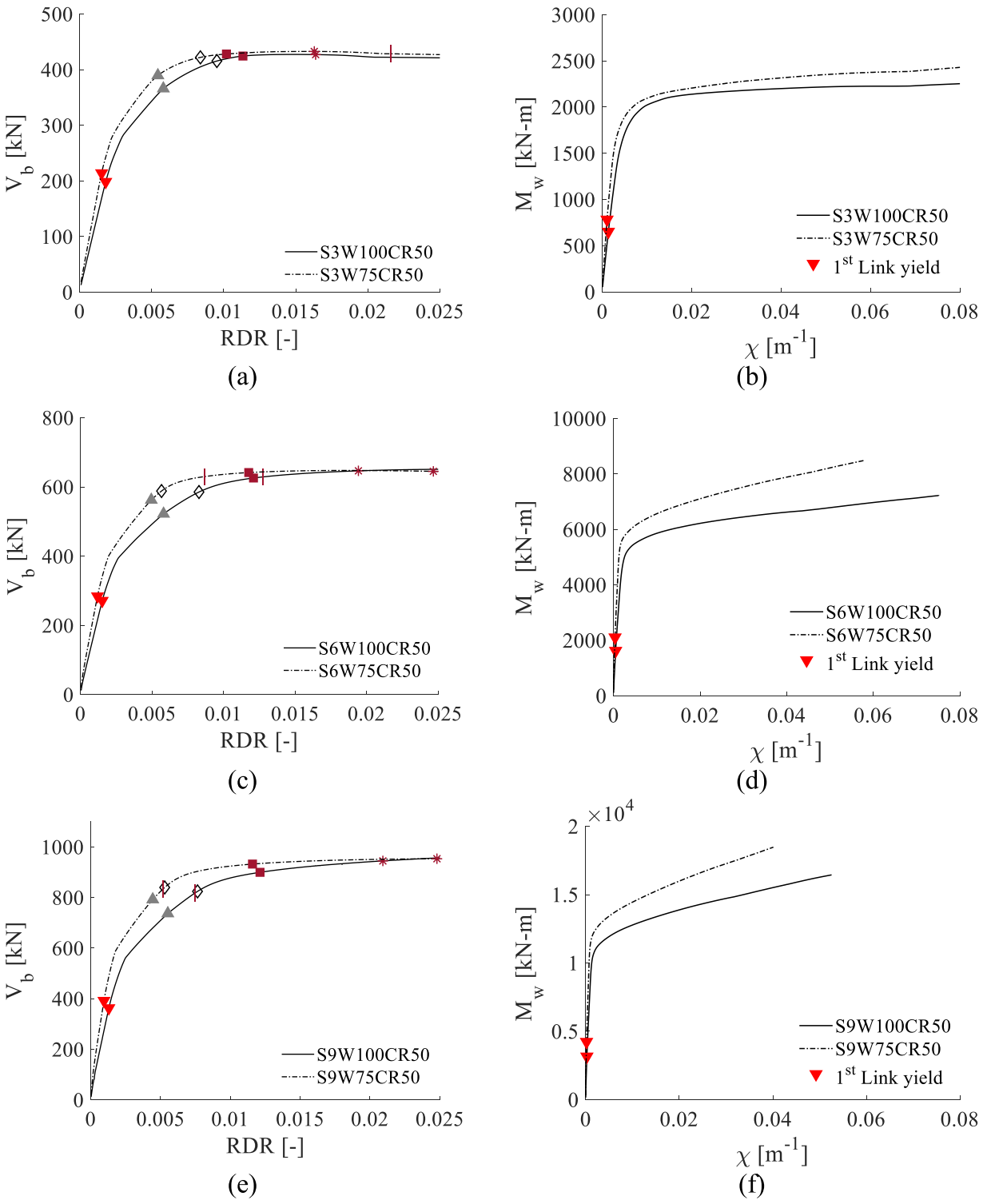

Fig. 13. Influence of the RC wall geometry (H/l_w ratio) in the fixed base designs: capacity curves (left-hand side) and moment-curvature response in the RC wall (right-hand side) for CR = 50 in the three-storey (a,b), six-storey (c,d), and nine-storey cases (e,f).

procedure and foster the possible use of SP-HCWs in real-world designs.

Author agreement statement

We the undersigned declare that this manuscript is original, has not been published before and is not currently being considered for publication elsewhere. We confirm that the manuscript has been read and approved by all named authors and that there are no other persons who satisfied the criteria for authorship but are not listed. We further confirm that the order of authors listed in the manuscript has been approved by all of us. We understand that the Corresponding Author is the sole contact for the Editorial process. He is responsible for communicating with the other authors about progress, submissions of revisions and final approval of proofs.

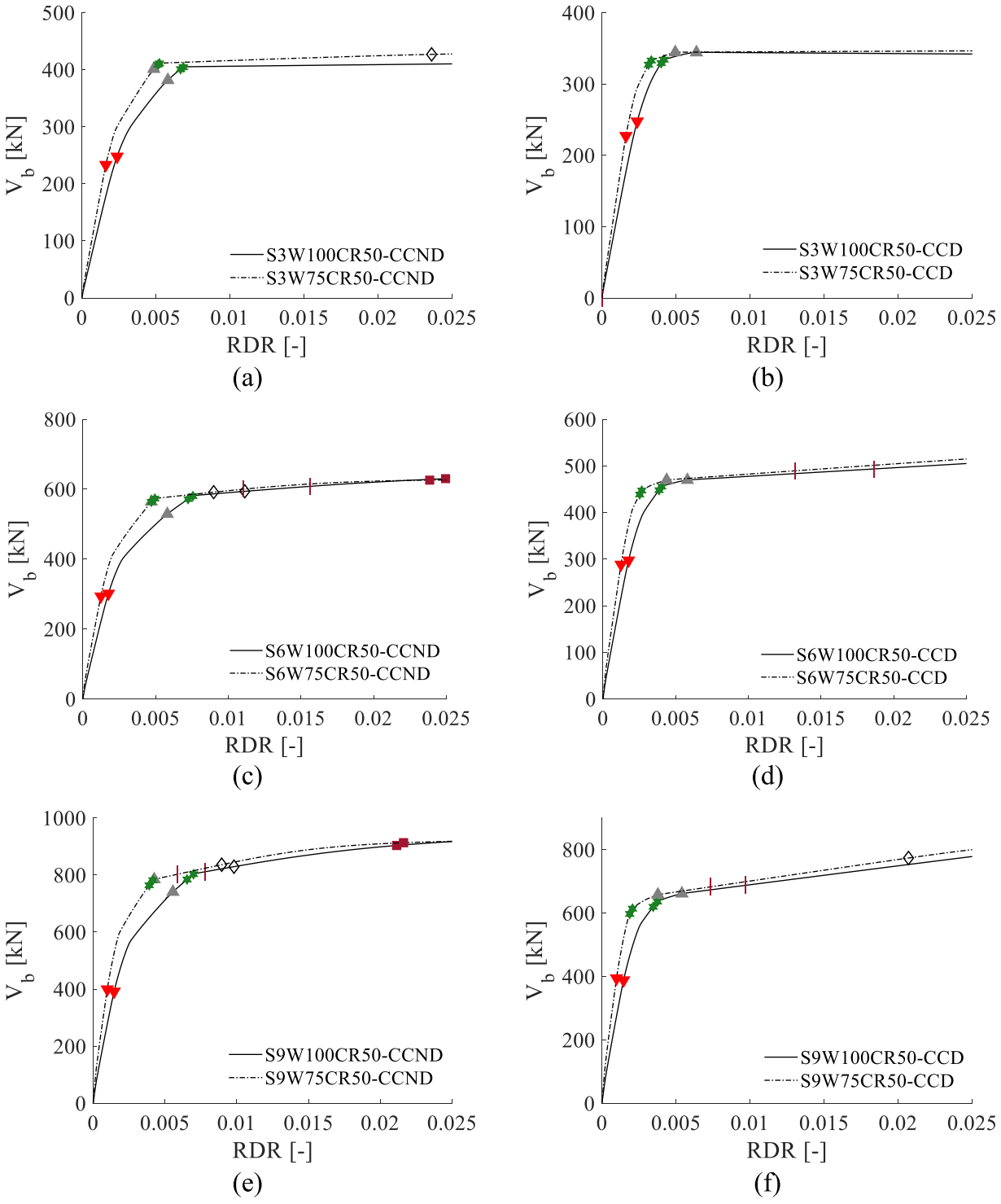

Fig. 14. Influence of the RC wall geometry (H/l_w ratio) in the hinged base designs: capacity curves for CR = 50 in the three-storey (a,b), six-storey (c,d), and nine-storey cases (e,f).

CRediT authorship contribution statement

Fabrizio Scozzese: Writing – review & editing, Writing – original draft, Visualization, Validation, Supervision, Software, Methodology, Investigation, Formal analysis, Data curation, Conceptualization. **Nicola Ceccolini:** Software, Formal analysis. **Alessandro Zona:** Writing – review & editing, Writing – original draft, Visualization, Validation, Supervision, Methodology, Investigation, Formal analysis, Data curation, Conceptualization. **Andrea Dall'Asta:** Resources, Project administration, Funding acquisition, Supervision, Conceptualization. **Hervé Degée:** Resources, Project administration, Funding acquisition, Conceptualization.

Declaration of Competing Interest

The authors declare that they have no known competing financial interests or personal relationships that could have appeared to influence the work reported in this paper.

Table 7
Ductility ratios in SP-HCWs with fixed base.

Label	μ_L	μ_D	μ_F	min (μ_D, μ_F)
S3W75CR40	3.0	6.0	14.0	6.0
S3W75CR50	3.5	5.5	13.5	5.5
S3W75CR60	5.0	5.0	13.5	5.0
S3W100CR40	2.5	5.5	18.0	5.5
S3W100CR50	3.0	5.5	18.5	5.5
S3W100CR60	4.0	4.5	17.0	4.5
S6W75CR40	3.0	4.5	6.0	4.5
S6W75CR50	4.0	5.0	7.0	5.0
S6W75CR60	4.5	4.0	5.5	4.0
S6W100CR40	3.0	6.0	8.0	6.0
S6W100CR50	4.0	5.5	8.0	5.5
S6W100CR60	4.0	4.0	6.5	4.0
S9W75CR40	4.0	6.0	5.5	5.5
S9W75CR50	4.5	5.5	5.0	5.0
S9W75CR60	6.0	4.5	5.0	4.5
S9W100CR40	3.5	7.0	6.0	6.0
S9W100CR50	4.0	6.0	5.5	5.5
S9W100CR60	5.0	5.0	5.0	5.0

Table 8
Ductility ratios in SP-HCWs with hinged base and non-dissipative corner components.

Label	μ_L	μ_D	μ_F	min (μ_D, μ_F)
S3W75CR40-CCND	2.5	13.5	18.0	13.5
S3W75CR50-CCND	3.0	14.5	18.0	14.5
S3W75CR60-CCND	3.5	16.0	18.0	16.0
S3W100CR40-CCND	2.0	11.5	19.0	11.5
S3W100CR50-CCND	2.5	13.5	19.5	13.5
S3W100CR60-CCND	3.0	15.5	18.5	15.5
S6W75CR40-CCND	3.0	6.5	7.5	6.5
S6W75CR50-CCND	4.0	7.5	8.5	7.5
S6W75CR60-CCND	4.0	6.5	7.5	6.5
S6W100CR40-CCND	2.5	6.0	8.0	6.0
S6W100CR50-CCND	3.5	6.5	8.5	6.5
S6W100CR60-CCND	4.0	7.0	8.0	7.0
S9W75CR40-CCND	4.5	5.0	5.0	5.0
S9W75CR50-CCND	4.5	9.0	5.5	5.5
S9W75CR60-CCND	5.0	9.0	5.5	5.5
S9W100CR40-CCND	3.0	7.0	5.0	5.0
S9W100CR50-CCND	4.0	6.5	5.0	5.0
S9W100CR60-CCND	4.5	7.0	5.0	5.0

Table 9
Ductility ratios in SP-HCWs with hinged base and dissipative corner components.

Label	μ_L	μ_D	μ_F	min (μ_D, μ_F)
S3W75CR40-CCD	2.0	25.0	17.5	17.5
S3W75CR50-CCD	3.0	31.0	20.5	20.5
S3W75CR60-CCD	3.5	26.0	16.5	16.5
S3W100CR40-CCD	2.0	20.0	20.0	20.0
S3W100CR50-CCD	2.5	21.0	21.0	21.0
S3W100CR60-CCD	3.0	22.0	19.5	19.5
S6W75CR40-CCD	3.0	19.0	9.0	9.0
S6W75CR50-CCD	3.5	22.0	10.0	10.0
S6W75CR60-CCD	3.5	18.5	8.5	8.5
S6W100CR40-CCD	2.5	19.0	9.5	9.5
S6W100CR50-CCD	3.5	21.0	10.0	10.0
S6W100CR60-CCD	4.0	21.5	9.0	9.0
S9W75CR40-CCD	3.5	21.0	7.0	7.0
S9W75CR50-CCD	4.0	21.0	7.0	7.0
S9W75CR60-CCD	4.5	19.0	6.0	6.0
S9W100CR40-CCD	3.0	18.0	6.5	6.5
S9W100CR50-CCD	3.5	17.5	6.0	6.0
S9W100CR60-CCD	4.5	17.5	5.5	5.5

Table 10
Mean values and coefficients of variations of the ductility ratios in SP-HCWs.

Base	Cases	Mean μ_L	Mean min (μ_D, μ_F)	COV μ_L	COV min (μ_D, μ_F)
Fixed	All	3.9	5.1	0.22	0.12
	CR 40	3.2	5.6	0.15	0.10
	CR 50	3.8	5.3	0.12	0.04
	CR 60	4.8	4.5	0.15	0.09
	3-storey	3.5	5.3	0.23	0.09
	6-storey	3.8	4.8	0.15	0.15
	9-storey	4.5	5.3	0.18	0.09
CCND	All	3.5	8.6	0.24	0.46
	CR 40	2.9	7.9	0.27	0.42
	CR 50	3.6	8.8	0.19	0.43
	CR 60	4.0	9.3	0.16	0.50
	3-storey	2.8	14.1	0.17	0.11
	6-storey	3.5	6.7	0.16	0.07
	9-storey	4.3	5.2	0.15	0.05
CCD	All	3.3	11.6	0.22	0.48
	CR 40	2.7	11.6	0.21	0.45
	CR 50	3.3	12.4	0.14	0.49
	CR 60	3.8	10.8	0.14	0.49
	3-storey	2.7	19.2	0.21	0.08
	6-storey	3.3	9.3	0.14	0.06
	9-storey	3.8	6.3	0.14	0.09

Data Availability

Data will be made available on request.

Acknowledgments

The results presented in this article were obtained within the research project “Innovative steel-concrete HYbrid Coupled walls for buildings in seismic areas: Advancements and Design guidelines” (HYCAD) funded by the European Commission, Research Fund for Coal and Steel (RFCS-RPJ: 899381). The support of the European Commission is gratefully acknowledged.

References

[1] Harries KA, Mitchell D, Cook WD, Redwood RG. Seismic response of steel beams coupling concrete walls. J Struct Eng 1993 1993;119(12):3611–29. https://doi.org/10.1061/(ASCE)0733-9445(1993)119:12(3611).
[2] Shahrooz BM, Remmetter MA, Quin F. Seismic design and performance of composite coupled walls. ASCE. J Struct Div 1993;19(11):3291–309. https://doi.org/10.1061/(ASCE)0733-9445(1993)119:11(3291).
[3] Harries KA, Gong B, Shahrooz BM. Behaviour and design of reinforced concrete, steel, and steel–concrete coupling beams. Earthq Spectra 2000;16(4):775–99. https://doi.org/10.1193/1.1586139.
[4] Park WS, Yun HD. Seismic behaviour of coupling beams in a hybrid coupled shear walls. J Constr Steel Res 2005;61(11):1492–524. https://doi.org/10.1016/j.jcsr.2005.04.006.
[5] El-Tawil S, et al. Seismic design of hybrid coupled wall systems: state of the art. J Struct Eng 2010;136(7):755–69. https://doi.org/10.1061/(ASCE)ST.1943-541X.0000186.
[6] Paulay T. Coupling beams of reinforced concrete shear walls. ASCE. J Struct Div 1971;97(3):843–62. https://doi.org/10.1061/JSDEAG.0002848.
[7] Paulay T, Santhakumar AR. Ductile behavior of coupled shear walls. ASCE. J Struct Div 1976;102(1):93–108. https://doi.org/10.1061/JSDEAG.0004279.
[8] Mahin SA, Bertero VV. Nonlinear seismic response of a coupled wall system. ASCE. J Struct Div 1976;102(9):1759–81. https://doi.org/10.1061/JSDEAG.0004428.
[9] Paulay T, Priestley MJN. Seismic Design of Reinforced Concrete and Masonry Buildings. New York: Wiley; 1992.
[10] Caprili S, Mussini N, Salvatore W. Experimental and numerical assessment of EBF structures with shear links. Steel Compos Struct 2018;28:123–38.

[11] Dall'Asta A, et al. Innovative Hybrid and Composite Steel-concrete Structural Solutions for Building in Seismic Area, Final Report. EUR 26932 EN. European Commission; 2015. https://doi.org/10.2777/85404.
[12] Zona A, Degeé H, Leoni G, Dall'Asta A. Ductile design of innovative steel and concrete hybrid coupled walls. J Constr Steel Res 2016;117(1):204–13. https://doi.org/10.1016/j.jcsr.2015.10.017.
[13] Das R, Zona A, Vandoren B, Degée H. Performance-based seismic design of an innovative HCW system with shear links based on IDA. Procedia Eng 2017;199(1):3516–21. https://doi.org/10.1016/j.proeng.2017.09.500.
[14] Zona A, Tassotti L, Leoni G, Dall'Asta A. Nonlinear seismic response analysis of an innovative steel and concrete hybrid coupled wall system. J Struct Eng 2018;144(7):04018082. https://doi.org/10.1061/(ASCE)ST.1943-541X.0002080.
[15] Das R, Zona A, Vandoren B, Degeé H. Optimizing the coupling ratio in the seismic design of HCW systems with shear dissipative links. J Constr Steel Res 2018;147(1):393–407. https://doi.org/10.1016/j.jcsr.2018.04.026.
[16] Salameh M, Shayanfar M, Barkhordari MA. Estimation and development of innovative hybrid coupled shear wall system using nonlinear dynamic and fragility analysis. Structures 2020;26(1):703–23. https://doi.org/10.1016/j.istruc.2020.04.031.
[17] Salameh M, Shayanfar M, Barkhordari MA. Seismic displacements and behaviour factors assessment of an innovative steel and concrete hybrid coupled shear wall system. Structures 2021;34(1):20–41. https://doi.org/10.1016/j.istruc.2021.07.058.
[18] Morelli F, Manfredi M, Salvatore W. An enhanced component based model for steel connection in a hybrid coupled shear wall structure: Development, calibration and experimental validation. Comput Struct 2016;176(1):50–69. https://doi.org/10.1016/j.compstruc.2016.08.002.
[19] Liu Q, Jiang H. Experimental study on a new type of earthquake resilient shear wall. Earthq Eng Struct Dyn 2017;46(14):2479–97. https://doi.org/10.1002/eqe.2914.
[20] Feng Y, Wu J, Chong X, Meng S. Seismic lateral displacement analysis and design of an earthquake-resilient dual wall-frame system. Eng Struct 2018;177(1):85–102. https://doi.org/10.1016/j.engstruct.2018.09.059.
[21] Wang W, Quan CC, Li Y, Zhen GK, Zhao HT. Experimental study and numerical simulation analysis on seismic performance of corrugated steel-plate shear wall with replaceable bottom corner dampers. Soil Dyn Earthq Eng 2022;152:107061. https://doi.org/10.1016/j.soildyn.2021.107061.
[22] Jiang Q, Zhou Y, Feng Y, Chong X, Wang H, Wang X, et al. Experimental study and numerical simulation of a reinforced concrete hinged wall with BRBs at the base. J Build Eng 2022;49(1):104030. https://doi.org/10.1016/j.jobe.2022.104030.
[23] Zhang Y, Xu LH. Experimental investigation of a new self-centering shear wall with resilient hinge devices. Eng Struct 2022;266(1):114657. https://doi.org/10.1016/j.engstruct.2022.114657.
[24] Zhang Y, Xu LH. Cyclic loading tests of a resilient hinged self-centering RC wall. Eng Struct 2022;270(1):114920. https://doi.org/10.1016/j.engstruct.2022.114920.
[25] Jiang Huanjun, Li Shurong, Bolander John E, Kunnath Sashi K. Seismic performance of a new type of coupled shear wall with replaceable components: experimental validation. J Earthq Eng 2022. https://doi.org/10.1080/13632469.2022.2033353.
[26] European Committee for Standardization, Eurocode 8: Design of structures for earthquake resistance - Part 1: General rules, seismic actions and rules for buildings. EN 1998–1, December 2004.
[27] Harries KA, McNeice DS. Performance-based design of high-rise coupled wall systems. Struct Des Tall Spec Struct 2006;15(3):289–306.
[28] Structural Engineering Institute. Recommendations for seismic design of hybrid coupled walls, ASCE, 2009. DOI: 10.1061/9780784410608.
[29] European Committee for Standardization, Eurocode 3: Design of steel structures - Part 1–1: General rules and rules for buildings. EN 1993–1-1, May 2005.
[30] European Committee for Standardization, Eurocode 2: Design of concrete structures - Part 1–1: General rules and rules for buildings. EN 1992–1-1, December 2004.
[31] McKenna F, Scott MH, Fenves GL. Nonlinear finite-element analysis software architecture using object composition. J Comput Civ Eng 2010;24(1):95–107. https://doi.org/10.1061/(ASCE)CP.1943-5487.0000002.
[32] Zona A, Dall'Asta A. Elastoplastic model for steel buckling-restrained braces. J Constr Steel Res 2012;68(1):118–25. https://doi.org/10.1016/j.jcsr.2011.07.017.
[33] Gu Q, Zona A, Peng Y, Dall'Asta A. Effect of buckling-restrained brace model parameters on seismic structural response. J Constr Steel Res 2014;98(1):100–13. https://doi.org/10.1016/j.jcsr.2014.02.009.
[34] Bosco M, Marino EM, Rossi PP. Modelling of steel link beams of short, intermediate or long length. Eng Struct 2015;84(1):406–18. https://doi.org/10.1016/j.engstruct.2014.12.003.